

Hadron production in central nucleus-nucleus collisions at chemical freeze-out

A. Andronic^a, P. Braun-Munzinger^a, J. Stachel^b

^a*Gesellschaft für Schwerionenforschung, D-64291 Darmstadt, Germany*

^b*Physikalisches Institut der Universität Heidelberg, D-69120 Heidelberg, Germany*

Abstract

We analyze the experimental hadron yield ratios for central nucleus-nucleus collisions in terms of thermal model calculations over a broad energy range, $\sqrt{s_{NN}}=2.7$ -200 GeV. The fits of the experimental data with the model calculations provide the thermal parameters, temperature and baryo-chemical potential at chemical freeze-out. We compare our results with the values obtained in other studies and also investigate more technical aspects such as a potential bias in the fits when fitting particle ratios or yields. Using parametrizations of the temperature and baryonic chemical potential as a function of energy, we compare the model calculations with data for a large variety of hadron yield ratios. We provide quantitative predictions for experiments at LHC energy, as well as for the low RHIC energy of 62.4 GeV. The relation of the determined parameters with the QCD phase boundary is discussed.

Key words: hadron production, statistical model, QCD phase diagram

1 Introduction

The success of the statistical (thermal) model [1] in describing the ratios of hadron yields produced in nucleus-nucleus collisions is remarkable. The thermal model was initially used for the AGS and SPS data [2] and was subsequently employed to describe data at SIS [3,4], SPS [5] and more recently at RHIC [6–9]. An analysis of the energy dependence of the thermal parameters extracted from fits of the experimental data, temperature (T) and baryo-chemical potential (μ_b), established the "line of chemical freeze-out" [10]. These data were subsequently interpreted in terms of an universal condition for chemical freeze-out [11]. Remarkably, it appears that at the top SPS energy the (T, μ_b) values reach the phase boundary between the hadronic world and the quark-gluon plasma (QGP) [1,10], as calculated solving Quantum Chromo-Dynamics (QCD) on the lattice [12–14]. In this context, it has been argued that the QGP itself and the "deus ex machina" of phase space filling during hadronization are playing the crucial roles in achieving thermalization in high energy nucleus-nucleus collisions [15]. More recently it was demonstrated that passing through the phase transition leads to multiparticle scattering of Goldstone bosons

which drives even (multi)strange baryons rapidly into equilibration [16], providing a natural explanation for the observation that the chemical freeze-out line reaches the phase boundary for small values of μ_b . The situation is less well understood for $\mu_b > 400$ MeV and needs further investigation.

Despite its simplicity, the thermal model allows to extract essential properties of the hot and dense fireball produced in high energy nucleus-nucleus collisions at a given stage in its evolution, namely when the inelastic collisions cease (chemical freeze-out). This makes the model a unique tool in the attempt to quantify from the experimental side the features of the phase diagram of hadronic matter [17–19]. Recent analyses over a broad energy range [20,21] have contributed in the on-going efforts to understand the chemical freeze-out criteria [1,10,11,22–24] in the phase diagram. It has been pointed out within a thermal model analysis that scanning the energy one encounters a transition from baryon- to meson-dominated freeze-out [25], with its associated fingerprint on the characteristics of hadron yields, also evidenced earlier [26].

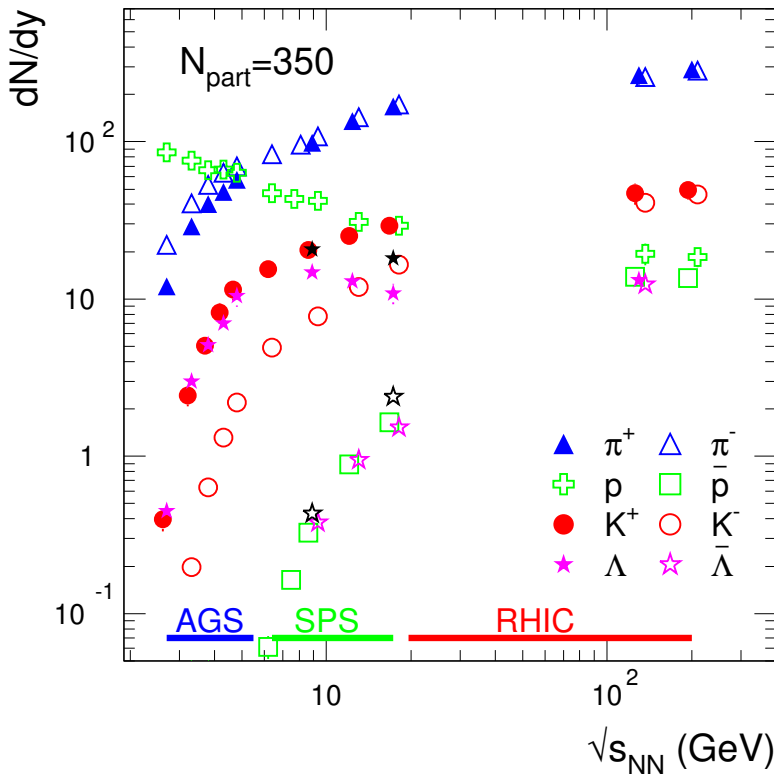


Fig. 1. The energy dependence of experimental hadron yields at mid-rapidity for various species produced in central nucleus-nucleus collisions. The energy regimes for various accelerators are marked. Note that, for SPS energies, there are two independent measurements available for the Λ hyperon yields. For more details see text (also in Section 3).

It is important to emphasize that experimental data on hadron yields are now available over a broad collision energy range and for a large sample of hadron species. A compilation of measurements of yields at mid-rapidity for the most abundant hadron species is shown in Fig. 1 for central nucleus-nucleus (Au-Au or Pb-Pb) collisions. As the centrality selection differs between various measurements, we have scaled the data at the same number of participating nucleons, $N_{part}=350$. The contribution from feeding due to weak decays has been removed whenever the case (see Section 3). The main properties concerning the chemical composition of the fireball (at mid-rapidity) can be derived from the yields plotted in Fig. 1 without the need of any model. At lower energies ($\sqrt{s_{NN}} \leq 5$ GeV), measured at Brookhaven’s Alternating Gradient Synchrotron (AGS), the fireball

is dominated by the incoming nucleons, while the yield of the produced pions, with a strong energy dependence, dominates at larger energies. The importance of isospin at lower energies is reflected in the different yields of π^+ and π^- . The decreasing yield of protons points to an increasing transparency of the incoming nuclei as a function of energy. Beyond $\sqrt{s_{NN}} \simeq 100$ GeV, the newly produced protons become dominant. The yield of strange hadrons shows a sharp rise at AGS energies, with characteristic features for various species, determined by their quark content. The yields of K^+ and Λ (both with only the strange quark newly produced) are larger compared to K^- , which has two newly produced quarks. The remarkable similarity of the yields of K^+ and Λ , despite their large mass difference, is determined chiefly by their (anti)strange quark content, leading to their associated production, and less by the abundant presence of light quarks from stopped incoming nucleons. The yield of antiprotons and antihyperons (containing three newly produced quarks) is very similar and with a strong energy dependence (onset of production) at energies of CERN's Super Proton Synchrotron (SPS). At the Relativistic Heavy Ion Collider (RHIC), due to a rather small net baryon content of the fireball, these differences almost disappear. The data are further discussed in Section 3 in comparison with thermal model calculations. We notice here that, in general, there is good consistency between overlapping data sets measured by different experiments. One exception are the hyperon yields at SPS energies, illustrated for Λ hyperons in Fig. 1.

In view of these considerations it is important to assess with precision potential uncertainties in the extraction of thermal parameters with a consistent, 2nd generation, analysis of all available experimental data over a broad range of collision energies ($\sqrt{s_{NN}}=2.7$ -200 GeV). This includes a comparison of the results from fits of hadron yield ratios and from absolute yields and a discussion on the influence of systematic errors on the fit parameters. The next section contains a brief description of the model. In Section 3 we perform fits of model calculations to the data. We discuss the energy dependence of the resulting T and μ_b parameters, along with a critical assessment of various sources of uncertainties, in Section 4. Section 5 is devoted to the comparison of model and data in terms of excitation functions of various hadron yield ratios, which we extend up to the LHC energy. The relation of the extracted parameters with the predicted QCD phase boundary, calculated solving QCD on the lattice [12–14], is discussed in Section 6. The Appendix contains a discussion of more technical aspects in the fit procedures.

2 Model description

We restrict ourselves here to the basic features and essential results of the statistical model approach. A complete survey of the assumptions and results, as well as of the relevant references, is available in ref. [1].

The basic quantity required to compute the thermal composition of hadron yields measured in heavy ion collisions is the partition function $Z(T, V)$. In the grand canonical (GC) ensemble, the partition function for species i is ($\hbar = c = 1$):

$$\ln Z_i = \frac{V g_i}{2\pi^2} \int_0^\infty \pm p^2 dp \ln[1 \pm \exp(-(E_i - \mu_i)/T)], \quad (1)$$

from which the density is then calculated according to:

$$n_i = N_i/V = -\frac{T}{V} \frac{\partial \ln Z_i}{\partial \mu} = \frac{g_i}{2\pi^2} \int_0^\infty \frac{p^2 dp}{\exp[(E_i - \mu_i)/T] \pm 1}, \quad (2)$$

where $g_i = (2J_i+1)$ is the spin degeneracy factor, T is the temperature and $E_i = \sqrt{p^2 + m_i^2}$ is the total energy. The (+) sign is for fermions and (-) is for bosons. For hadron i of baryon number B_i , third component of the isospin I_{3i} , strangeness S_i , and charmness C_i , the chemical potential is $\mu_i = \mu_b B_i + \mu_{I_3} I_{3i} + \mu_S S_i + \mu_C C_i$. The chemical potentials related to baryon number (μ_b), isospin (μ_{I_3}), strangeness (μ_S) and charm (μ_C) ensure the conservation (on average) of the respective quantum numbers: i) baryon number: $V \sum_i n_i B_i = N_B$; ii) isospin: $V \sum_i n_i I_{3i} = I_3^{tot}$; iii) strangeness: $V \sum_i n_i S_i = 0$; iv) charm: $V \sum_i n_i C_i = 0$. The (net) baryon number N_B and the total isospin I_3^{tot} of the system are input values which need to be specified according to the colliding nuclei studied. The degree of stopping of the colliding nuclei, which is energy dependent and cannot be precisely determined experimentally, brings some uncertainty in the choice of N_B and I_3^{tot} . In our case, as we study central collisions of heavy nuclei (Au or Pb), but focus on data at mid-rapidity, we have chosen $N_B=200$ and $I_3^{tot}=-20$. The sensitivity of the hadron ratios, which are the calculated "observables" to be compared with the experimental data, on N_B and I_3^{tot} is rather small. Taking into account the conservation laws i)-iv), T and the baryo-chemical potential μ_b are the only parameters of the model, which will be obtained from fits to experimental data. When fitting hadron yields rather than ratios of yields, the fireball volume appears as additional parameter. We discuss its physical significance in Section 4 and in the Appendix.

We want to emphasize that our model does not contain any strangeness suppression factor, γ_S , as used e.g. in ref. [20,21]. Whenever γ_S is used in thermal model calculations¹, it is meant to account for non-equilibration in the strangeness sector. Departure from equilibrium is expected for elementary collisions or for peripheral nucleus-nucleus collisions (as well as for light nuclei). The introduction of a γ_S factor is an attempt to model this situation (see e.g. [27,20]). It is established that $\gamma_S \simeq 1$ for central collisions at RHIC [8,9]. At the lower end of the energy range, namely at SIS energies (up to 2 AGeV), there are indications [3] that γ_S is not needed either. As we investigate central Au-Au or Pb-Pb collisions we prefer to stay within the thermodynamically well defined equilibrium model. Nevertheless we investigate, in the Appendix, the influence on our results as well as the statistical significance of the introduction of γ_S into the fit procedure. This leads to the conclusion that our main results, i.e. the determination of T and μ_b from fits of ratios of yields at mid-rapidity, are little changed by this additional fit parameter.

The following hadrons are included in the calculations: i) mesons: non-strange (37), strange (28), charm (15), bottom (16); ii) baryons: non-strange (30), strange (33), charm (10); iii) "composites" (nuclei up to ^4He and K^- -clusters [28], 18). The corresponding anti-particles are of course also included. Their characteristics, including a rather complete set of decay channels, (all strong decays and a suitable fraction of the weak decays contribution matching the experimental conditions) are implemented according to the

¹ We recall that the usage of γ_S implies that the thermal density of any given hadron carrying strangeness has a "suppression" factor γ_S for every strange or antistrange quark.

most recent PDG compilation [29]. Studies of QCD thermodynamics using lattice results have demonstrated that the partition function of a hadron and resonance gas model, which is a sum over all individual partition functions (Eq. 1), describes the lattice QCD data after suitably rescaling hadron masses to match lattice QCD [30].

We have used vacuum masses for all hadrons. The effect of hadron mass (and width) modification was analyzed in the context of the thermal model for the top SPS energy in ref. [31]. The conclusion is that at SPS a 10% reduction of masses leads to a slightly better thermal fit, with a corresponding 10% reduction of the resulting T and μ_b . A thermal analysis of the RHIC data using hadron masses derived from chiral models [32] found no preference for any scenario of in-medium masses compared to the non-interacting gas model. Note that at AGS (Si+Au) the nominal masses are preferred [1]. It was argued [33,34] that changes of masses in-medium in connection to chiral symmetry restoration can lead to larger values of the chemical potentials at lower energies.

The finite widths of resonances are taken into account in the density calculation by an additional integration, over the particle mass, with a Breit-Wigner distribution as a weight:

$$n_i = \frac{g_i}{2\pi^2} \frac{1}{N_{BW}} \int_{M_0}^{\infty} dm \int_0^{\infty} \frac{\Gamma_i^2}{(m - m_i)^2 + \Gamma_i^2/4} \cdot \frac{p^2 dp}{\exp[(E_i^m - \mu_i)/T] \pm 1}, \quad (3)$$

where m_i is the nominal mass and Γ_i is the width of particle i . The energy is then calculated for every value of m in the integration step, $E_i^m = \sqrt{p^2 + m^2}$. Here, N_{BW} is the normalization of the Breit-Wigner distribution and M_0 is the threshold for the dominant decay channel. As this procedure significantly increases the computing time, for the fits it was used only for the AGS energies (see below), where in particular the widths of nucleon resonances are expected to play a significant role [35]. At higher energies the width of the resonances plays little role in the determination of the thermal parameters.

The interaction of hadrons and resonances is usually included by implementing a hard core repulsion of Van der Waals-type via an excluded volume correction. This is implemented in an iterative procedure according to ref. [36,37]:

$$P^{excl.}(T, \mu) = P^{id.gas}(T, \hat{\mu}); \quad \hat{\mu} = \mu - V_{eigen} P^{excl.}(T, \mu) \quad (4)$$

where V_{eigen} is calculated for a radius of 0.3 fm, considered identical for all hadrons [5]. This correction influences the particle densities, but has little (<5%) effect on ratios. The effect on absolute densities is very significant, however: at top SPS energies and above the excluded volume procedure leads to a reduction in densities by about a factor of 2, leading to a correspondingly larger volume at chemical freeze-out.

The grand canonical ensemble is the simplest realization of a statistical approach and is suited for systems with a large number of produced hadrons. However, for small systems (or peripheral nucleus-nucleus collisions) and for low energies in case of strangeness production, a canonical ensemble (C) treatment is mandatory [38]. It leads to a phase space reduction for particle production (so-called ‘‘canonical suppression’’). It has been shown [39,1] that the density of particle i with strangeness S calculated in the canonical

approach, n_i^C , is with a good approximation related to the grand canonical value, n_i^{GC} , as: $n_i^C = n_i^{GC}/F_S$, with $F_S = I_0(x)/I_S(x)$. The argument of the Bessel function of order S is the total yield of strange and antistrange hadrons. The suppression factor is shown in Fig. 2 for a canonical volume $V_C=1000 \text{ fm}^3$, which we employ in our calculations (see next section). In this case, the canonical suppression is negligible for all strange hadron species already for the highest AGS energy ($\sqrt{s_{NN}} \simeq 5 \text{ GeV}$) but is sizeable for the lower energies. Whenever the canonical suppression is needed, V_C , becomes another parameter of the model and needs to be evaluated carefully (see below).

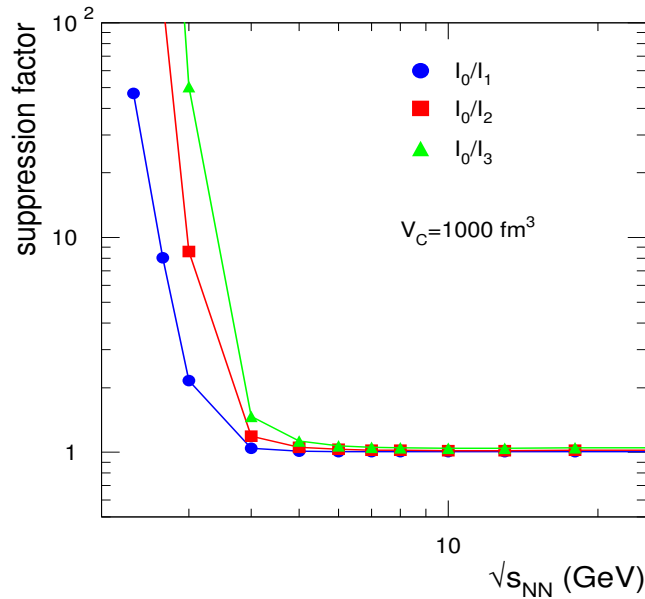


Fig. 2. The energy dependence of the canonical suppression factor for strangeness, calculated for the canonical volume $V_C=1000 \text{ fm}^3$.

We mention that several similar codes are now available for thermal model calculations: SHARE [40], THERMUS [41], Therminator [42].

3 Fits to experimental data

To extract the parameters of the model we perform fits of the experimental data with model calculations. In order to employ a minimal number of model parameters, namely T and μ_b , the temperature and the baryonic chemical potential at chemical freeze-out (ceasing of inelastic collisions), a common practice is to fit hadron yield ratios [1,7–9]. It is important to recognize that one is faced with a choice when selecting $N - 1$ statistically independent ratios from the total number $N(N - 1)/2$ of ratios which can be constructed from N experimentally measured hadron yields. Although the number of independent hadron yields is typically rather large ($N > 10$) one may argue that fitting a particular choice of (statistically independent) particle ratios may introduce a bias for the extracted T and μ_b whenever a given experimental yield used in several ratios is subject to a systematic error. To minimize such a possible bias, we use ratios constructed from

all measured hadron species avoiding, as much as possible, the repetition of any particular yield. Another possibility is to fit the measured hadron yields [20,21], which implies an extra parameter, the fireball volume. This method is free of the bias discussed above, but is subject of another bias, arising, for instance, whenever two measured yields (i.e. of a particle and its antiparticle) have a similar systematic error, which is cancelled in the ratio. Also, ratios typically have a smaller systematic error than absolute yields. Based on this, our main analysis focusses on ratios of hadron yields. As mentioned in Section 4 and demonstrated in detail in the Appendix, the difference of fit parameters resulting from the two different fit procedures is always smaller than the uncertainty in the overall method, given the current status of measured yields and corresponding errors.

We briefly discuss below the fit procedures. The best fit is obtained by minimizing the distribution of χ^2 . To get an estimate of the systematic error of the fits, we additionally consider the quadratic deviation, δ^2 . The two quantities are defined as:

$$\chi^2 = \sum_i \frac{(R_i^{exp} - R_i^{therm})^2}{\sigma_i^2}, \quad \delta^2 = \sum_i \frac{(R_i^{exp} - R_i^{therm})^2}{(R_i^{therm})^2}, \quad (5)$$

where R_i^{exp} is the measured value of either the yield or the ratio of hadron yields² with its uncertainty σ_i and R_i^{therm} is the value from the model calculations. For the experimental errors we have quadratically added the statistical and the systematic errors of the measured yields. When the systematic errors of the measurements were not available we have assigned values of 10%, unless otherwise stated. The sum runs over the number of hadron ratios available experimentally. We focus on central collisions of Au or Pb nuclei. Ratios are calculated from the measured hadron yields. Whenever needed, we scale the measured yields with the number of participants [43] to account for different centrality classes.

We focus on mid-rapidity data (dN/dy), for which the bulk of the published hadron yields is available, but we also analyze data integrated over the full solid angle whenever available. While at low energies the consideration of hadron yields integrated over 4π is optimal, this changes as, with increasing beam energy, the nuclei become transparent and, besides a central fireball, fragmentation regions develop. Once the stopping is not complete, necessarily the baryo-chemical potential depends on rapidity and a consideration of 4π data with one value of μ_b would not be appropriate. In that case the statistical model should be compared to data over a central region near mid-rapidity. One may consider in separate analyses more forward or backward fireballs with different parameters. The possible presence of a finite net strangeness at mid-rapidity, as suggested by a recent transport model calculation [44], could pose a special difficulty; this is not accounted for in our model. However, the effect is expected to be small enough to not cause a systematic bias of the extracted thermal parameters.

An important aspect in the comparison of calculations with measurements is the contribution of feed-down from weak decays, mainly in the yields of pions and (anti)protons. In our model, the fraction of those hadrons originating from weak decays is adjusted. In general, this contribution is subtracted in the experiments, either explicitly (via simu-

² We denote a yield ratio of two particles by the ratio of their respective symbols.

lations) or implicitly (due to specific reconstruction methods). We have tried to model in detail the contributions from weak decays, following the information in the relevant experimental papers. In the Appendix we demonstrate the importance to determine as precisely as possible the size of this contribution.

3.1 AGS

At the AGS, collisions of Au nuclei at beam kinetic energies of 2 to 10.7 AGeV, corresponding to $\sqrt{s_{NN}}=2.70$ -4.85 GeV were studied. For the beam energies of 2, 4, 6, and 8 AGeV, the yields of protons [45,46], pions [47,48] and kaons [48] are available (there are no K^- data at 2 AGeV). The Λ yields are only available integrated over 4π [49] and for the energy of 6 AGeV the integrated Ξ^- yield was also measured [50]. In these cases we have derived the mid-rapidity values assuming the same ratio between 4π and dN/dy as for protons [45].

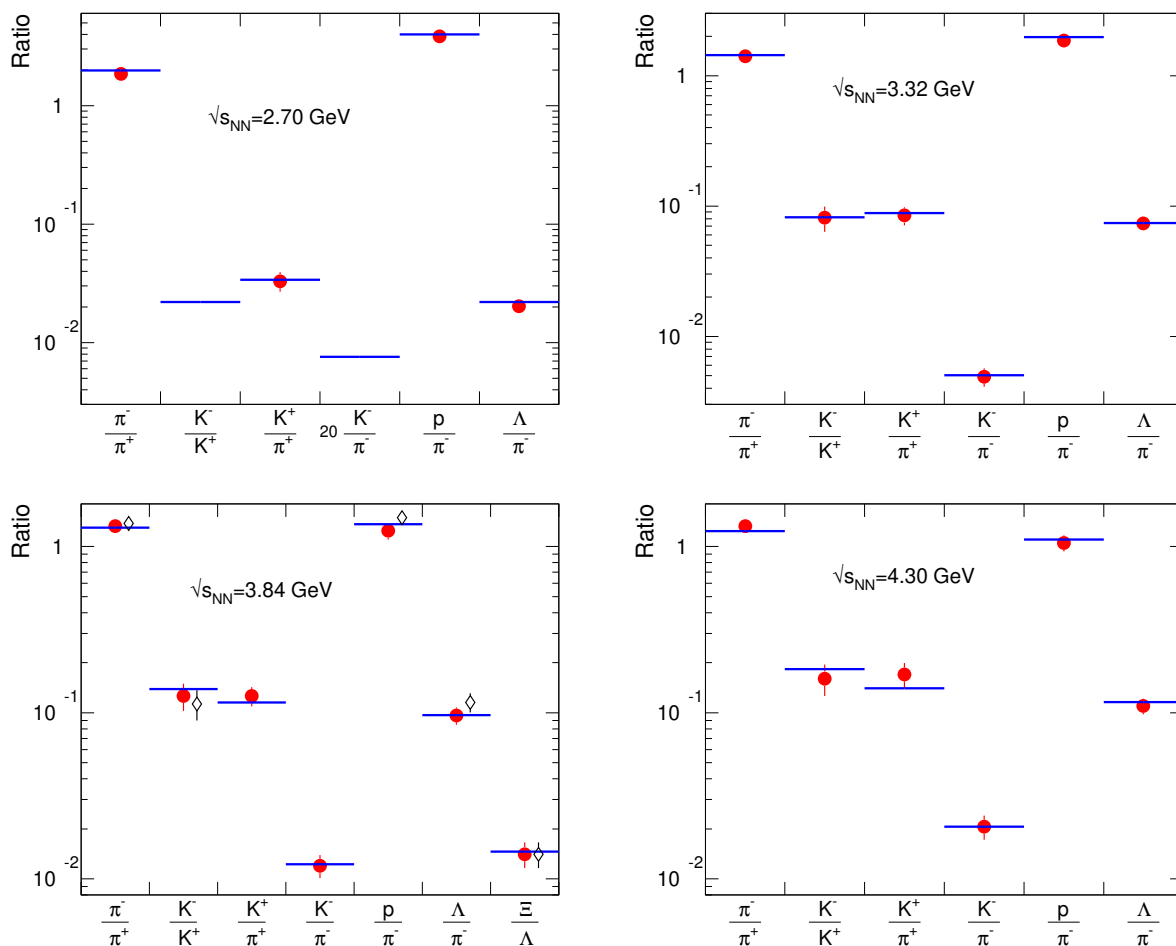


Fig. 3. Measured hadron yield ratios compared to the thermal model calculations for the AGS beam energies of 2, 4, 6, and 8 AGeV. The symbols are data, the lines are model calculations corresponding to the best fit (T, μ_b) values of (64,760), (78,670), (86,615), and (93,580) MeV, respectively. For the beam energy of 6 AGeV the ratios of 4π yields are plotted as diamonds.

The comparison of the measured and calculated ratios for the best fit (χ^2 minimization) is presented in Fig. 3 for the four energies. Here and in the following plots we show both

the K^+/π^+ and the K^-/π^- ratios, but in the fit either one or the other is included (as only one is statistically independent from the ratios π^-/π^+ and K^-/K^+), depending on the minimum value of χ^2 . The resulting values of T and μ_b are between 64 and 93 MeV and 760 and 580 MeV, respectively. The model describes the data very well; the χ^2 values per number of degrees of freedom, χ^2/N_{df} are 1.0/2, 0.43/3, 1.15/4, 1.14/3 for 2, 4, 6, and 8 AGeV, respectively. Although this could be accidental, as the number of data points in the fits is very small, these low values could imply that the systematic errors of the measurements are actually overestimated. We mention that if we do not include in the calculations the finite widths of resonances the corresponding values of χ^2/N_{df} are slightly worse, but the values of T and μ_b change only marginally. For both cases, the χ^2 distributions are narrow around the minimum and there is no correlation between T and μ_b as is observed for higher energies (see below). In some cases, close-by minima are identified and we have included this feature into the errors of the parameters.

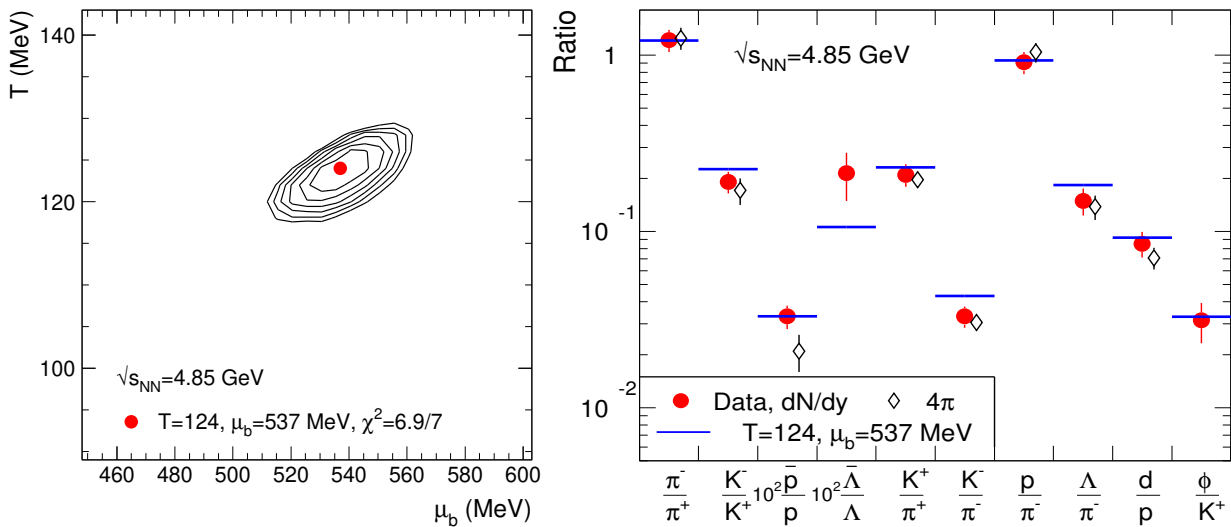


Fig. 4. The χ^2 contours (in steps of 1 from the minimum, marked by the dot) and yield ratios with best fit at mid-rapidity for the top AGS beam energy of 10.7 AGeV. The diamonds represent ratios of yields integrated over 4π . The ratio K^-/π^- was not included in the fit. Note the scaling factor of 100 for the ratios \bar{p}/p and $\bar{\Lambda}/\Lambda$.

At the top AGS beam kinetic energy of 10.7 AGeV ($\sqrt{s_{NN}}=4.85$ GeV) there is a large set of hadron yields experimentally available: p [51,52,46], d [52], π [51,48], K [48,53], Λ [54], ϕ [55], $\bar{\Lambda}$ [56]. The thermal fit to the data yields $T = 124 \pm 3$ MeV and $\mu_b = 537 \pm 10$ MeV, corresponding to a minimum of $\chi^2/N_{df}=6.9/7$ (the errors correspond to 1σ). The model fits the data very well, as evident from the narrow χ^2 distribution and from the comparison of the ratios shown in Fig. 4. Not included in the fit is the ratio K^-/π^- , which is not statistically independent from the ratios already included in the fit. The ratio $\bar{\Lambda}/\Lambda$ deviates from the model calculations substantially ($\bar{\Lambda}$ "anomaly" [56]). The experimental $\bar{\Lambda}/\Lambda$ is a factor of 2 higher than the model value and as such has a significant contribution to the χ^2 (if $\bar{\Lambda}/\Lambda$ is not included in the fit, the resulting values are: $T = 123 \pm 3$ MeV, $\mu_b = 538 \pm 9$ MeV, $\chi^2/N_{df}=4.0/6$).

The fit without the ratios d/p , \bar{p}/p , $\bar{\Lambda}/\Lambda$, and ϕ/K^+ gives $T = 108 \pm 9$, $\mu_b = 555 \pm 18$

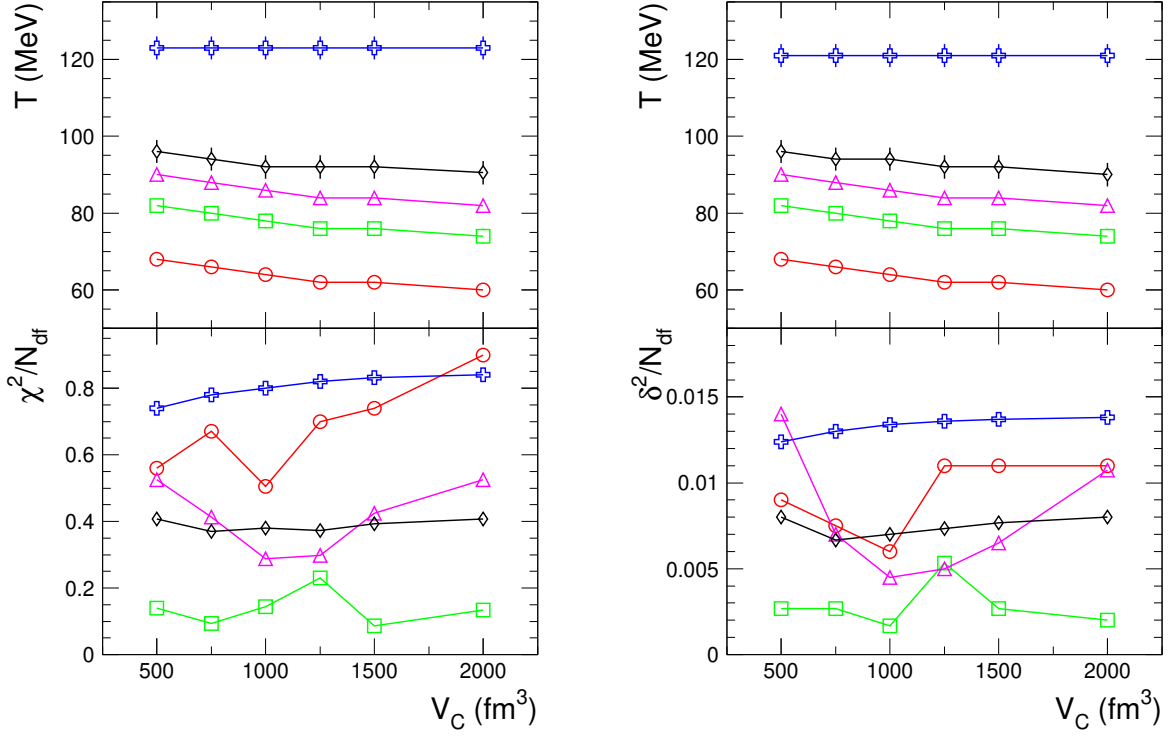


Fig. 5. The canonical volume dependence of temperature extracted from thermal fits for the AGS beam kinetic energies of 2, 4, 6, 8, and 10.7 AGeV (in order of increasing temperature). Left panel is for minimizing χ^2 , right panel is for δ^2 . The corresponding χ^2/N_{df} and δ^2/N_{df} are also shown.

MeV, with $\chi^2/N_{df}=1.3/3$. We note that, in this case, T and μ_b are not anymore correlated (as seen in Fig. 4), but rather loosely anticorrelated. We have performed this fit to test a possible bias in the extracted thermal parameters at the lower energies due to the smaller number of ratios experimentally available. We estimate in this way that the extracted temperature can be biased by up to 15%, while for μ_b the bias can be up to 3%. These systematic (upper limits) errors are used in the following.

To investigate the sensitivity of the extracted (T, μ_b) values on the canonical volume V_C (which enters via the canonical suppression factor), we have performed the fits for all AGS energies for a range of V_C values. The results are presented in Fig. 5, where we show the dependence of T on the canonical volume parameter V_C for two cases: minimizing χ^2 and δ^2 . Both cases result in very similar freeze-out temperatures. As expected, T slightly grows with decreasing V_C . The effect is gradually reduced towards higher energies and totally vanishes at the top AGS energy. Based on the dependence of χ^2/N_{df} and δ^2/N_{df} on V_C (also shown in Fig. 5) one cannot constrain the canonical volume parameter. As a consequence, and since the canonical volume dependence is a rather small effect, we have chosen the value $V_C=1000 \text{ fm}^3$. We mention that μ_b is unaffected by the canonical volume choice.

3.2 SPS

At the CERN SPS Pb-Pb collisions are measured in fixed target experiments, with beam momenta (\approx energies) of 20 to 158 AGeV ($\sqrt{s_{NN}}=6.27-17.3$ GeV). For the time being only the data collected at 40, 80 and 158 AGeV are final. The mid-rapidity yields of pions, kaons and (anti)protons and deuterons [57–60] are available for these energies. The yields of the complete set of strange (anti)hyperons [61–65] and of ϕ [66] are published for the top energy and at 40 AGeV. Since the deuteron yield is measured over a reduced range in momentum, we have decided to not include the deuterons in the fitting procedure for all the SPS energies, although the ratio d/p will be shown in the following plots. Also shown in the plots are the ratios Ξ/π^- and Ω/π^- , which are not included in the fits because they are not independent from the ratios Ξ/Λ and Ω/Ξ , respectively, which are used because they result in a better fit.

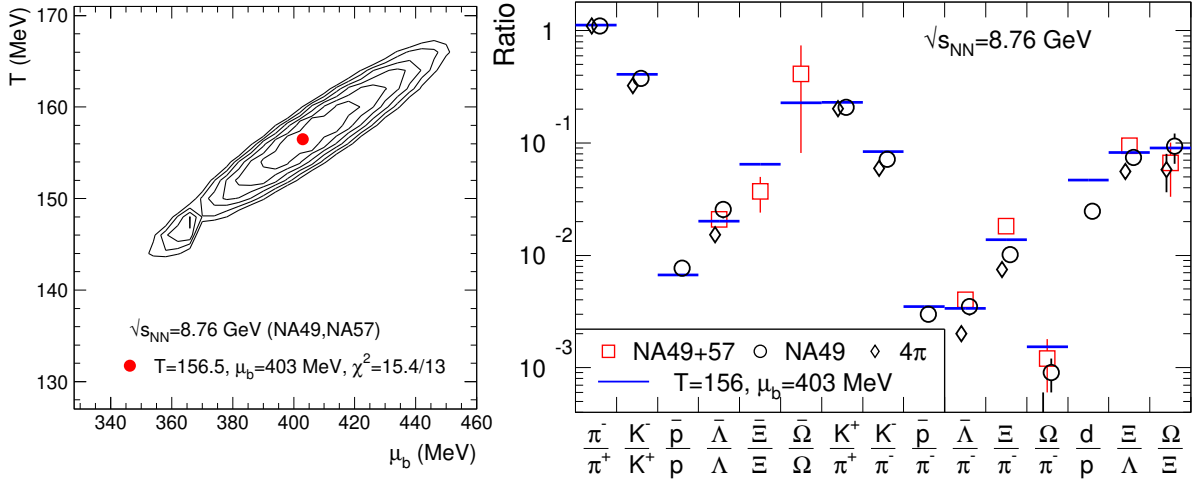


Fig. 6. Distribution of χ^2 and hadron yield ratios with best fit at the SPS beam energy of 40 AGeV using the NA49 and NA57 mid-rapidity data (the ratios K^-/π^- , d/p , Ξ/π^- and Ω/π^- are not included in the fits). The NA49 4π data are plotted for comparison (diamonds). For the ratios Ω/π^- and Ω/Ξ , the Ω yield includes both Ω and $\bar{\Omega}$.

At the beam energy of 40 AGeV ($\sqrt{s_{NN}}=8.76$ GeV), a combined fit to all data gives $T=156_{-3}^{+4}$ MeV, $\mu_b=403_{-14}^{+18}$ MeV, with $\chi^2/N_{df}=15.4/13$ (from the quadratic deviation analysis, $T=166$ MeV, $\mu_b=434$ MeV, $\delta^2=0.58$). The χ^2 distribution and the comparison of the measured and calculated ratios for the best fit are shown in Fig. 6. A fit of NA49 data alone leads to $T=166\pm 2$ MeV, $\mu_b=438\pm 7$ MeV, with $\chi^2/N_{df}=6.2/7$ ($T=162$ MeV, $\mu_b=414$ MeV, $\delta^2=0.10$).

The χ^2 distribution and the comparison of the measured and calculated ratios for the beam energy of 80 AGeV ($\sqrt{s_{NN}}=12.3$ GeV) are shown in Fig. 7. The best fit is achieved for $T=154$ MeV, $\mu_b=298$ MeV, with 1σ errors of 6 and 20 MeV, respectively ($T=152$ MeV, $\mu_b=271$ MeV, with minimum $\delta^2=0.23$). The quality of the fit is not good, as seen from the value of $\chi^2/N_{df}=23.4/5$. We have noticed that the outcome of the fit is sensitive to the inclusion of different (statistically equivalent) hadron ratios. For instance, if the ratios

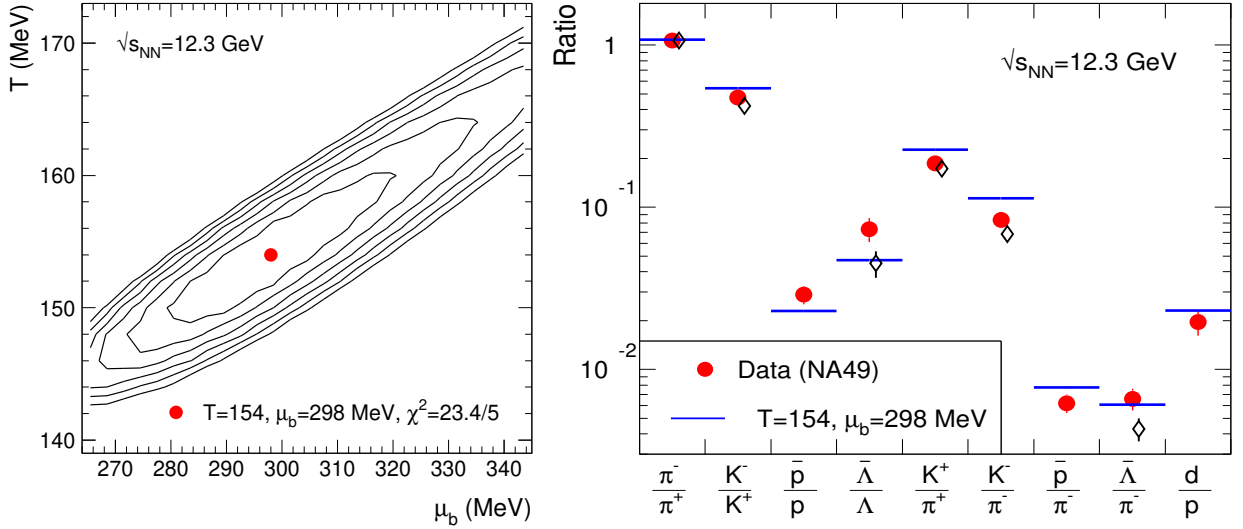


Fig. 7. Distribution of χ^2 and hadron yield ratios with best fit at the beam energy of 80 AGeV using the NA49 data (the ratios K^-/π^- and d/p were not included in the fit). The 4π yields (represented with diamonds) are plotted for comparison.

p/π^- and Λ/π^- are considered instead of \bar{p}/π^- and $\bar{\Lambda}/\pi^-$ the resulting temperature from χ^2 minimization is lower by about 10 MeV, while the temperature from δ^2 minimization is unchanged. This shows the effect of the errors on the outcome of the χ^2 minimization and indicates that the errors of the data are not entirely consistent. We have incorporated these results into the systematic errors of the thermal parameters.

For the top SPS energy of 158 AGeV ($\sqrt{s_{NN}}=17.3$ GeV), there are mid-rapidity measurements available from the experiments NA49 [58,59,61–63], NA57 [64,65] (hyperons and K_S^0) and NA44 [57] (π , K , p). Note that the NA44 pion yields are not explicitly corrected for the contribution from weak decays, but this is estimated to be small if one takes into account the reconstruction procedure in the NA44 spectrometer [67]. We have assumed an efficiency of reconstruction of 40% for pions from K_S^0 (considered the average yield of K^+ and K^- measured by NA44) and of 20% from Λ (considered the average of the NA57 and NA49 yields) decays. In this way, 5.9 π^+ and 7.8 π^- (dN/dy) are estimated to originate from weak decays.

We have used in the fits the ratios Ξ/Λ and Ω/Ξ . This choice leads to better values of χ^2 compared to the case when using the ratios Ξ/π^- and Ω/π^- instead. The ratio d/p was not included in the fits. The measured and calculated ratios for the best fit are shown in Fig. 8. A fit to all the combined NA49, NA57 and NA44 data gives $T = 160 \pm 5$ MeV and $\mu_b = 240 \pm 18$ MeV, with $\chi^2/N_{df}=56/22$ (from the least square deviation minimization, $T=172$ MeV, $\mu_b=243$ MeV, $\delta^2=0.86$). For instance, if the ratios Ξ/π^- and Ω/π^- are considered instead of Ξ/Λ and Ω/Ξ , $T = 155 \pm 2$ MeV and $\mu_b = 224 \pm 6$ MeV, with $\chi^2/N_{df}=63/22$ ($T=170$ MeV, $\mu_b=237$ MeV, $\delta^2=1.03$).

To investigate the contribution to these large values of χ^2/N_{df} , we have considered separately two sets of hadron ratios:

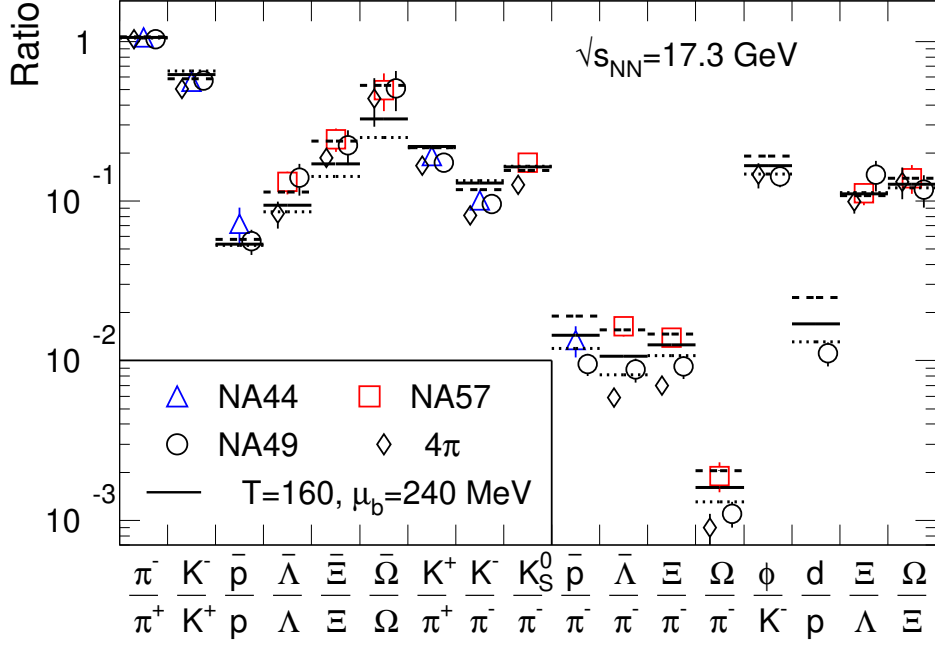


Fig. 8. The ratios of hadron yields at mid-rapidity with best fits at the top SPS energy of 158 AGeV. For the ratios of hyperons and K_S^0 from NA57 relative to pions, we have used the π^- yields measured by NA44. The 4π ratios with NA49 data (diamonds) are plotted for comparison. The full lines are for the combined fit, the dashed ones for the NA44+NA57 data ($T=180$, $\mu_b=268$ MeV) and the dotted ones for the NA49 data ($T=150$, $\mu_b=266$ MeV). The ratios K^-/π^- , d/p , Ξ/π^- and Ω/π^- are not included in the fit.

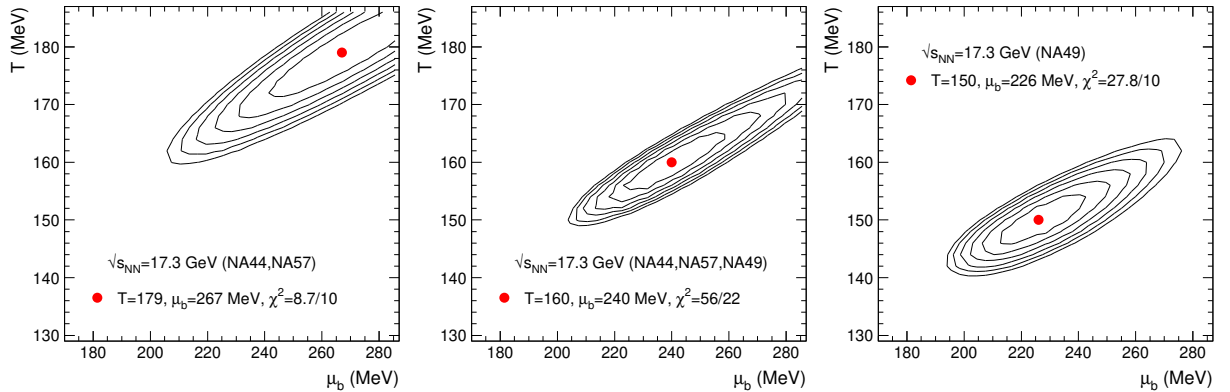


Fig. 9. The χ^2 distributions at the top SPS energy of 158 AGeV for three cases (see text).

i) the combined NA57 and NA44 data³ give $T = 179 \pm 7.5$ MeV and $\mu_b = 267 \pm 26$ MeV. With $\chi^2/N_{df}=8.7/10$, the fit quality is good.

³ In combining data from different experiments we neglect the possible difference in centralities at the same quoted fraction of the inelastic cross section which may arise from different centrality measures.

ii) using the NA49 data we extract $T = 150 \pm 4.5$ MeV, $\mu_b = 226 \pm 15$ MeV, with $\chi^2/N_{df}=27.8/10$. The fit quality is much worse compared to the NA57 and NA44 data set.

The χ^2 contours for the combined fit and for the two separate data sets are shown in Fig. 9. The outcome of the fits is summarized in Table 1. While μ_b is compatible within the errors for all the three cases, the value of the temperature differs significantly, well beyond the errors, between the NA49 and the NA44+NA57 data sets. This discrepancy imposes large systematic errors for the extracted thermal parameters (see next section). Remarkably, the values extracted from the δ^2 minimization are very similar for all three cases, $T \simeq 170$ MeV, $\mu_b \simeq 240$ MeV. This indicates that the outcome of the combined fit is driven by the NA49 data and in particular by their small errors. Although unsatisfactory thermal fits may signal a possible change in physics in connection to the critical (end)point of a first order phase transition from hadrons to QGP [68], the experimental situation just discussed allows unfortunately no conclusion on this issue. The apparent inconsistency of the results obtained using two independent data sets is not alleviated if one uses in the fit hadron yields instead of ratios. The results for this case (presented in Table 4 in the Appendix) show a similar pattern as in case of the fits using ratios. We note that poor quality of the fits at SPS energies characterizes other recent analyses within the thermal model [20,69].

Table 1

Summary of the results of the fits using mid-rapidity data at top SPS energy ($\sqrt{s_{NN}}=17.3$ GeV). The first three and next three columns show the results of the χ^2 (with their 1σ error) and δ^2 minimization, respectively.

data set	T (MeV)	μ_b (MeV)	χ^2/N_{df}	T (MeV)	μ_b (MeV)	δ^2
NA44+NA57	179 ± 7.5	267 ± 26	8.7/10	174	243	0.15
NA49	150 ± 4.5	226 ± 15	27.8/10	168	240	0.66
combined	160 ± 5	240 ± 18	56/22	172	243	0.86

3.3 RHIC

A complete set of final data for Au-Au collisions at RHIC is available at $\sqrt{s_{NN}}=130$ GeV. We use for our analysis the yields of pions, kaons, (anti)protons [70] and Λ , $\bar{\Lambda}$ [71] measured by PHENIX, while for the other hadron species, Ξ , Ω [72,73], ϕ [74], K^* [75], the data are from STAR. Most of the available data are not corrected for feed-down from weak decays, but these contributions are properly taken into account in the model calculations. One exception are the pions, for which the weak decay feed-down contribution is not clearly specified by the experiment (PHENIX). We have considered three cases:

- i) Assuming that all the pions from feed-down are included in the data, the values of the thermal parameters are $T = 170.5 \pm 6$ MeV and $\mu_b = 38 \pm 15$ MeV, with a minimum χ^2/N_{df} value of 3.6/11.
- ii) At the other extreme, if one considers that the pion data do not contain any contribution from weak decays, the resulting values are $T = 162.5 \pm 5.5$ MeV, $\mu_b = 35 \pm 11$ MeV, $\chi^2/N_{df}=4.6/11$.
- iii) Assuming that the data contain 30% of the pions from weak decays, $T = 165.5 \pm 5.5$

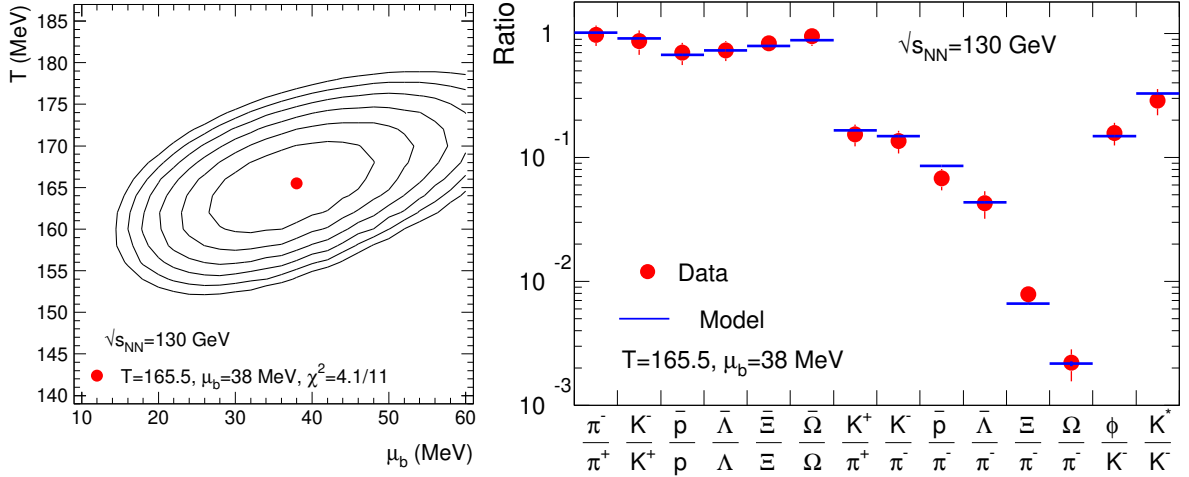


Fig. 10. The χ^2 distribution and hadron yield ratios with best fit at $\sqrt{s_{NN}}=130$ GeV. Here, the Ω yield includes both Ω and $\bar{\Omega}$.

MeV, $\mu_b = 38 \pm 11$ MeV, $\chi^2/N_{df}=4.1/11$.

Although the fit is good for all cases (and even if the minimal χ^2 is obtained for case i), we consider the intermediate case iii) as the most likely situation, as it could be an implicit result of the reconstruction in the experiment. The outcome of the fit is shown in Fig. 10. The very good fit is also apparent in the comparison of the hadron ratios: essentially all the experimental ratios are well reproduced by the model, including those involving ϕ and K^* resonances.

At $\sqrt{s_{NN}}=200$ GeV only a limited set of yields of identified hadrons is available to date. The yields of π^\pm , K^\pm , p , and \bar{p} are published by PHENIX [76], STAR [77], and BRAHMS [78] and the values agree within the quoted systematic errors. In addition, available are the yields of ϕ [79,80], $K(892)^*$ [81], d and \bar{d} [82]. We use the hadron ratios with the corresponding errors whenever provided by the experiments [76,79–81] or otherwise calculate the ratios using the published yields quoted above. Further ratios are available as preliminary data on strange hyperon ratios [83], Δ^{++}/p [84], \bar{p}/π^- , $\bar{\Lambda}/\pi^-$, Ξ/π^- , Ω/π^- , and Λ^*/Λ [85]. Unless specified, our fits do not include the ratios involving resonances (Δ^{++}/p , $K(892)^*$, and Λ^*).

We consider the following cases for the fits:

i) a combined fit of all available data, with the exception of strongly decaying resonances: $T = 155 \pm 2$ MeV, $\mu_b = 26 \pm 5$ MeV, $\chi^2/N_{df} = 34.1/23$ (with δ^2 minimization: $T=164$ MeV, $\mu_b=24$ MeV, $\delta^2=0.40$). If we include in the fit the three ratios involving resonances (K^*/K^- , Λ^*/Λ , and Δ^{++}/p), the results are the same within the errors, $T = 155 \pm 2$ MeV, $\mu_b = 25 \pm 5$ MeV, but with a worse $\chi^2/N_{df} = 41.8/26$ ($T=162$ MeV, $\mu_b=22$ MeV, $\delta^2=0.82$).

ii) as i), but excluding from the fit the ratios \bar{p}/π^- and ϕ/K^- from PHENIX. The resulting parameters are: $T = 160.5 \pm 2$ MeV, $\mu_b = 20 \pm 4$ MeV, with $\chi^2/N_{df}=16.0/21$ ($T=166$ MeV, $\mu_b=26$ MeV, $\delta^2=0.19$). Including the resonances the outcome of the fit is identical, $T = 160 \pm 2$ MeV, $\mu_b = 20 \pm 4$ MeV, with a reasonable $\chi^2/N_{df} = 25.2/24$ ($T=164$ MeV,

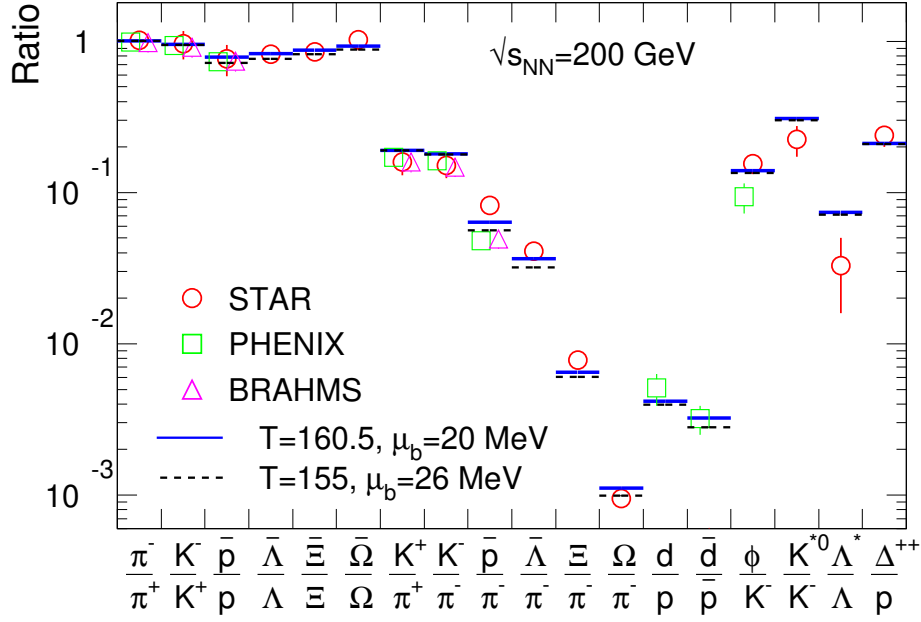


Fig. 11. Hadron yield ratios with best fits at $\sqrt{s_{NN}}=200$ GeV (see text). The last three ratios, involving resonances, were not included in the fits.

$\mu_b=20$ MeV, $\delta^2=0.61$).

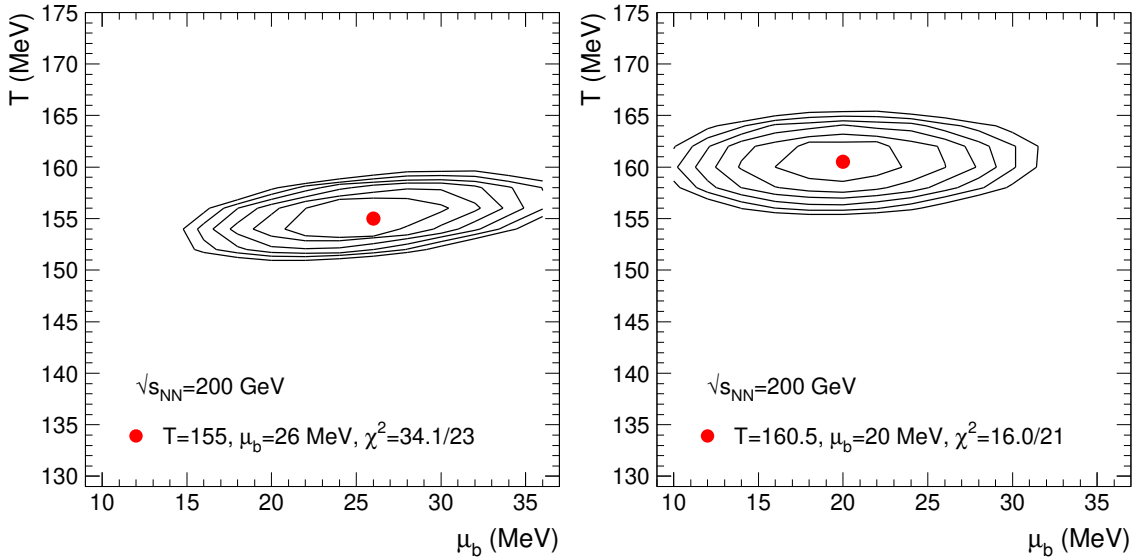


Fig. 12. Distributions of χ^2 at $\sqrt{s_{NN}}=200$ GeV for the two cases in Fig. 11: a combined fit of all available data (left panel) and excluding the ratios \bar{p}/π^- and ϕ/K^- from PHENIX (right panel).

Obviously, the outcome of the fit (lower T) for case i) is determined by two contributions:

a) the 6% systematic error assigned by PHENIX to the ratio \bar{p}/π^- , which is much smaller than the values 14% and 18% which we calculate from the systematic errors of the absolute yields in case of BRAHMS and STAR data, respectively; b) the ratio ϕ/K^- from PHENIX [80], which is much lower compared to the value from STAR [79]. Using all data from STAR (without resonances) and the d/p and \bar{d}/\bar{p} ratios from PHENIX gives $T = 160.5 \pm 2$ MeV, $\mu_b = 15 \pm 7$ MeV, with $\chi^2/N_{df} = 11.6/13$ (from δ^2 minimization: $T=166$ MeV, $\mu_b=22$ MeV, $\delta^2=0.17$). Taking into account that, for all cases, the δ^2 minimization results lead to $T > 160$ MeV, and despite the fact that the χ^2/N_{df} is reasonable even for the global fit, we consider the fit without the ratios \bar{p}/π^- and ϕ/K^- from PHENIX (case ii) as the nominal case for $\sqrt{s_{NN}}=200$ GeV. The systematic errors are then estimated as the differences to the case when all measured hadrons (but no resonances) are included in the fit and to the values from the δ^2 minimization.

The experimental ratios and the best fit calculations for the two cases, i) and ii) are shown in Fig. 11. Their respective χ^2 distributions are shown in Fig. 12. We note that, comparing the resonances, only the Λ^* ratio is clearly deviating from the model fits in our case, at variance with other claims in this respect [86]. Despite this deviation, which needs further support from the experimental side, our results on resonances do not point to a sizeable hadronic rescattering effect after chemical freeze-out [86].

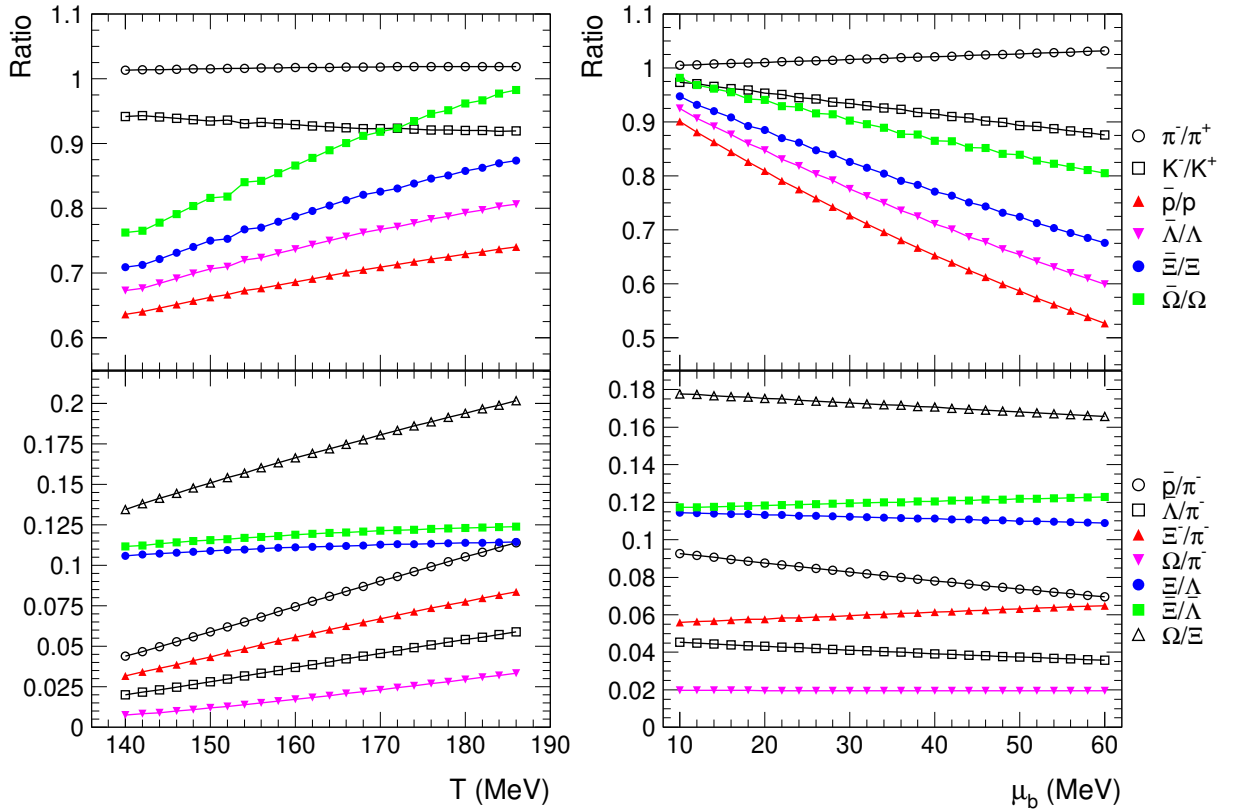


Fig. 13. The dependence of various hadron ratios on T and μ_b for the range of parameters relevant for the RHIC energies. Note that the ratios Ξ^-/π^- and Ω^-/π^- are scaled up by a factor 10.

In Fig. 13 we show the sensitivity of various hadron ratios on T and μ_b for the range

of values relevant for the RHIC energies [6]. The importance of particular ratios in constraining T and/or μ_b is evident. The antihyperon to hyperon ratios as well as the ratios of heavy hadrons to pions are of special value in this respect.

We note that thermal models have also been used to describe hadron production in e^+e^- and hadron-hadron collisions [38,27], leading to temperature parameters in the range 160-170 MeV. We mention that our model does not fit well the e^+e^- data. Our fits to the data at $\sqrt{s_{NN}}=29$ GeV compiled in ref. [27] were performed constraining $\mu_b=0$ and with three free parameters: the temperature, T , the strangeness suppression factor, γ_S , and the volume, V (used to calculate the canonical suppression factor). The fits yield $T = 154 \pm 3$ MeV, $\gamma_S = 0.74 \pm 0.06$ and $V = 42 \pm 14$ fm³, with a $\chi^2/N_{df}=56/11$. Obviously, the fit quality is very poor. For comparison, in the analysis of ref. [27] $T = 159 \pm 2.6$ MeV, $\gamma_S = 0.71 \pm 0.05$, $\chi^2/N_{df}=29.3/12$. Both T and μ_b are compatible within the errors, but our fit shows a much worse quality. This may be due to the approximations concerning canonical strangeness suppression which are employed in the present approach. However, even with the appropriate canonical treatment as done in ref. [27], the quality of the fits (both in e^+e^- and in hadron-hadron collisions) is not good, raising questions about the applicability of the statistical model for elementary collisions.

4 Energy dependence of the thermal parameters

Our results for the best fits are summarized in Table 2. The upper part in Table 2 shows the results of the fits using mid-rapidity data, the lower part is for the data integrated over 4π . One notices that in general χ^2/N_{df} is close to (and often below) unity, being significantly above unity only for the SPS energies. The fits 4π -integrated data result in comparable temperature values as for the mid-rapidity data in case of the AGS energies and sizably lower values for the SPS energies. For the higher SPS energies, the fits of 4π data are characterized by even poorer χ^2 values. We would like to stress that, although we have performed the fits of 4π data up to the top SPS energy (in order to compare to similar analyses in other works), we consider the extracted thermal parameters in this case adequate only up to the energy of 40 AGeV. Also included in Table 2 are the results of the δ^2 minimization, which differ sometimes from those obtained from the χ^2 minimization. The central values used in the following are those from the χ^2 minimization.

The "systematic" errors ΔT^{syst} and $\Delta \mu_b^{syst}$ shown in Table 2 are obtained by quadratically adding the 1σ error from the χ^2 minimization with the difference between the values obtained by χ^2 and δ^2 minimization. Whenever redundant sets of data are available from different experiments, which is the case at top SPS and top RHIC energies, our "nominal" values are those resulting from the combined fit of all data. We have assigned as systematic error the quadratic sum of 1σ fit errors and the deviation between the (T, μ_b) values of this case and those resulting from the fit of the data which results in the smallest value of χ^2 (see previous section and Table 2). For the SPS energy of 80 AGeV ($\sqrt{s_{NN}}=12.4$ GeV) the systematic errors are evaluated based on the sensitivity of the fit on the inclusion of different hadron ratios. As discussed in the previous section, for lower AGS beam energies of 2-8 AGeV, we have estimated 14% and 3% systematic errors for T and μ_b , respectively, based on the sensitivity of the fit using ratios at top AGS energy. For the AGS energy

Table 2

Summary of the results of the thermal fits using ratios. The upper part shows the results obtained using mid-rapidity data, the lower part is for data integrated over 4π . The first three and next three columns show the results of the χ^2 (with their 1σ error) and δ^2 minimization, respectively. The quantities ΔT^{syst} and $\Delta\mu_b^{syst}$ (in MeV) are the assigned systematic errors (see text).

$\sqrt{s_{NN}}$ (GeV)	T (MeV)	μ_b (MeV)	χ^2/N_{df}	T	μ_b	δ^2	ΔT^{syst}	$\Delta\mu_b^{syst}$
2.70	64±1	760±20	1.0/2	64	760	0.012	+10,-2	23
3.32	78±2	670±16	0.43/3	78	670	0.005	+12,-3	20
3.84	86±2	615±8	1.15/4	86	615	0.018	+13,-3	19
4.30	93±3	580±11	1.14/3	94	580	0.021	+14,-3	17
4.85	124±3	537±10	6.9/7	130	540	0.34	7	12
8.76	156 $^{+4}_{-3}$	403 $^{+18}_{-14}$	15.4/13	166	434	0.61	11	32
12.3	154±6	298±19	23.4/5	152	271	0.23	12	33
17.3	160±5	240±18	55/22	172	243	0.86	+19,-12	24
130	165.5±5.5	38±11	4.1/11	168	42	0.12	6	11
200	160.5 ±2	20±4	16.0/21	166	22	0.19	6	7
3.84	86.5±2	631±11	6.7/4	88	640	0.14	12	19
4.85	115±4	535±11	9.0/5	116	530	0.15	5	15
6.27	132.5±3	518±15	4.4/4	136	516	0.13	5	16
7.62	138±3	459±12	22/4	140	449	0.22	7	19
8.76	135±5	380±19	32/5	142	387	0.21	9	22
12.3	146.5±3.3	316±17	30/4	144	277	0.13	4	39
17.3	151±9	256±41	36/9	170	285	0.39	+18,-5	41

of 6 AGeV, we have used the available 4π yields of pions [47], protons [45], Λ and K_S^0 [49]. We note that, at this energy, there are no K^+ and K^- yields measured in full phase space. Based on a comparison of the ratio K^-/K^+ at mid-rapidity and in 4π at top AGS energy [53], we have assumed that at 6 AGeV the ratio K^-/K^+ in 4π is 10% smaller than at mid-rapidity. At the top AGS energy, some of the 4π yields do not correspond to complete coverage [53]; also, the ratio \bar{p}/p is obtained with a rather large extrapolation.

In Fig. 14 we show the energy dependence of T and μ_b extracted from our thermal fits. The temperature T exhibits a sharp rise up to $\sqrt{s_{NN}} \simeq 7-8$ GeV, while μ_b sharply decreases all the way up to RHIC energies. Our results are compared with results from other studies [1,3,8,20,21,69], which exhibit similar trends. One notable exception are the results of Letessier and Rafelski [21]; in this case, the observed difference may arise from the usage in their work of seven free parameters, including, besides strangeness fugacity and suppression factor (γ_S), a light quark occupancy factor (γ_q) and an isospin fugacity. The non-monotonic change in γ_q and γ_S as a function of energy determines the temperature extracted in ref. [21]. To alleviate the poor quality of the fits at SPS energies, the model of Dumitru et al. [69], introducing an inhomogeneous freeze-out scenario, goes beyond other thermal models.

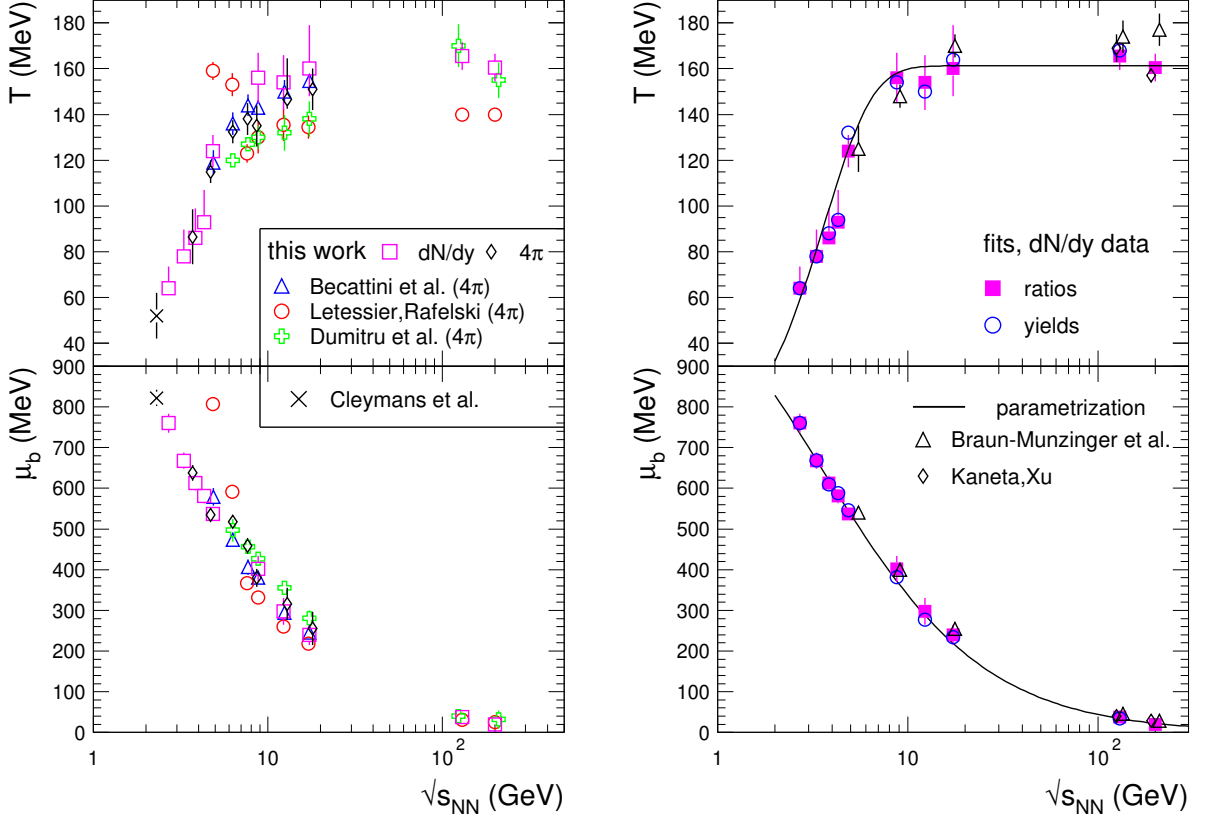


Fig. 14. The energy dependence of temperature and baryon chemical potential. Left panel: the results of the present work are compared to the values obtained in earlier studies (see text); right panel: the results of our fits using dN/dy data, both with ratios and yields. The lines are parametrizations for T and μ_b (see text).

Not surprisingly, our results support those obtained earlier within the same model implementation [1]. In detail, there are differences between our results and the rest of the other results. Our values for the analysis of the 4π data are significantly different from those of Becattini et al. [20], obtained within a model employing the strangeness suppression factor. A remarkable agreement between our results and the analyses in ref. [6,8] is seen in case of the RHIC data, in particular at $\sqrt{s_{NN}}=130$ GeV. The results at $\sqrt{s_{NN}}=200$ GeV [8,9] are also in agreement with our values. The higher T value at $\sqrt{s_{NN}}=200$ GeV in ref. [6] is due to preliminary data.

We have parametrized our results from the fits of mid-rapidity data (left panel in Fig. 14 and Table 2) as a function of $\sqrt{s_{NN}}$ (in GeV) with the following expressions:

$$T[\text{MeV}] = T_{lim} \left(1 - \frac{1}{0.7 + (\exp(\sqrt{s_{NN}}(\text{GeV})) - 2.9)/1.5} \right) \quad (6)$$

$$\mu_b[\text{MeV}] = \frac{a}{1 + b\sqrt{s_{NN}}(\text{GeV})}, \quad (7)$$

where the parameters $a = 1303 \pm 120$ MeV and $b = 0.286 \pm 0.049$ GeV $^{-1}$ are the results of

a fit ($\chi^2/N_{df}=0.48/8$). Our μ_b parametrization is the one proposed in ref. [26], but with different parameters to better fit the newly obtained μ_b values of the present analysis. In Eq. 6 we assume a "limiting" temperature T_{lim} , which was obtained by fitting the five points for the highest energies (SPS and RHIC). The result of the fit is $T_{lim} = 161 \pm 4$ MeV, with $\chi^2/N_{df}=0.3/3$.

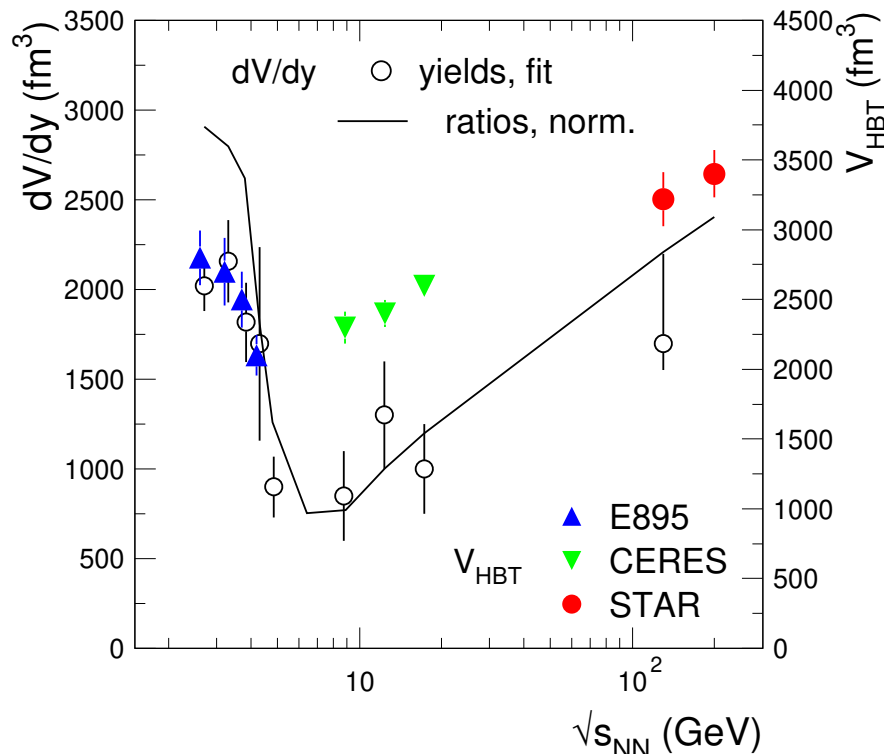


Fig. 15. Energy dependence of the volume for central collisions ($N_{part}=350$). The chemical freeze-out volume for one unit of rapidity, dV/dy , is compared to the kinetic freeze-out volume from HBT measurements, V_{HBT} [87]. Note that the scales are different for the two observables.

We now briefly turn to another interesting parameter which is (either implicitly or explicitly) determined in the course of thermal model analyses. The volume at chemical freeze-out (corresponding to a slice of one unit of rapidity, dV/dy) is shown in Fig. 15 as a function of energy. The values extracted directly from the fits of particle yields (see Appendix) are compared to the values obtained by dividing measured charged particle yields with calculated densities (based on the above parametrization of T and μ_b ; note that for the AGS energies of 2-8 AGeV the values of T corresponding to the upper limit of the systematic error were used instead). As expected, the two methods give identical results, with the exception of a small discrepancy for the lowest energies. The chemical freeze-out volume is compared to the kinetic freeze-out volume extracted from Hanbury Brown and Twiss (HBT) measurements, V_{HBT} [87]. We note here (see also the Appendix) that to determine a volume from thermal model analyses one needs to know absolute densities. This implies an explicit dependence of the volume on whether or not excluded volumes are implemented in the calculations, and, if included, on details of the implementation. We follow here the procedure developed in [5].

While the bias towards unphysically large volumes seen at the energies of 2-8 AGeV (see

Appendix) is not completely understood, it is clear that the volume at kinetic freeze-out should not be exceeded. Note that, to relate quantitatively the magnitude of the rapidity density of the chemical freeze-out volume dV/dy to the volume at kinetic freeze-out determined from HBT measurements, one needs to map rapidity onto space (see the discussion in [87]). Here we are mainly interested in the energy dependence of the two volumes. It appears that the volume at chemical freeze-out does exhibit a similar non-monotonic behavior as the volume at kinetic freeze-out, a remarkable result considering that the latter is determined by a completely different procedure. A minimum is observed for the top AGS energy, followed by a logarithmic increase as a function of $\sqrt{s_{NN}}$.

5 The energy dependence of hadron ratios

Using the parametrizations of the chemical freeze-out parameters derived from the fits of experimental data at mid-rapidity, as shown in Eq. 6 and 7, we calculate the energy dependence of various hadron ratios. No contribution from weak decay feed-down is included in the model calculations as the published data are mostly corrected in this respect. Whenever not the case, the measurements are scaled appropriately (see below). The finite widths of resonances are taken into account in the model. This contributes about 10% of pions at low energies and 4% at higher energies. Within the smoothing hypothesis implied by the parametrizations of Eq. 6 and 7, the model has interpolative and extrapolative predictive power. In this sense, we can provide quantitative predictions for LHC energy, as well as for the low RHIC energy of 62.4 GeV, for which the experimental data are becoming available [88]. This also applies to the low energy SPS data [89].

In Fig. 16 we show the energy dependence of antiparticle to particle ratios. Calculations employing the global $T(\sqrt{s_{NN}})$ and $\mu_b(\sqrt{s_{NN}})$ from Eq. 6 and 7 reproduce very well all these experimental ratios, including the preliminary values for $\sqrt{s_{NN}}=62.4$ GeV [88]. The π^-/π^+ , K^-/K^+ , and \bar{p}/p ratios illustrate the decreasing importance of isospin, the increasing importance of strangeness production and the dramatic evolution as a function of energy of the balance between the incoming and newly produced protons. The ratio \bar{p}/p has the steepest dependence on energy. From the lowest measured value of $3 \cdot 10^{-4}$ at AGS, it reaches a value of about 0.7 at RHIC and is predicted to reach 0.95 at LHC. The dominance of the initial nucleons at low energies changes to the newly created hadrons at RHIC and beyond. At LHC, it is expected that the fireball will consist practically completely of created hadrons ($\mu_b \simeq 1$ MeV).

The energy dependence of antihyperon/hyperon ratios (right panel in Fig. 16) follows a mass hierarchy: the saturation value of 1 is achieved the earlier the more massive the hyperon species. This is a fingerprint of the preferred abundance of hyperons over antihyperons containing 2 (Λ) or 1 (Ξ) light valence quarks, which may be remnants from the incoming nucleons, while in case of Ω , all valence quarks are newly produced.⁴ Remarkably, as already seen in Fig. 8, there is a very good agreement between the NA49 [61–63] and the NA57 [64] data. The ratio $\bar{\Lambda}/\Lambda$ from the NA45 (CERES) experiment [90]

⁴ The small structure of the excitation function at $\sqrt{s_{NN}}=10-20$ GeV, most prominently seen in Fig. 16 for the ratio $\bar{\Omega}/\Omega$, but also for $\bar{\Xi}/\Xi$, is an artifact of our parametrization of μ_b .

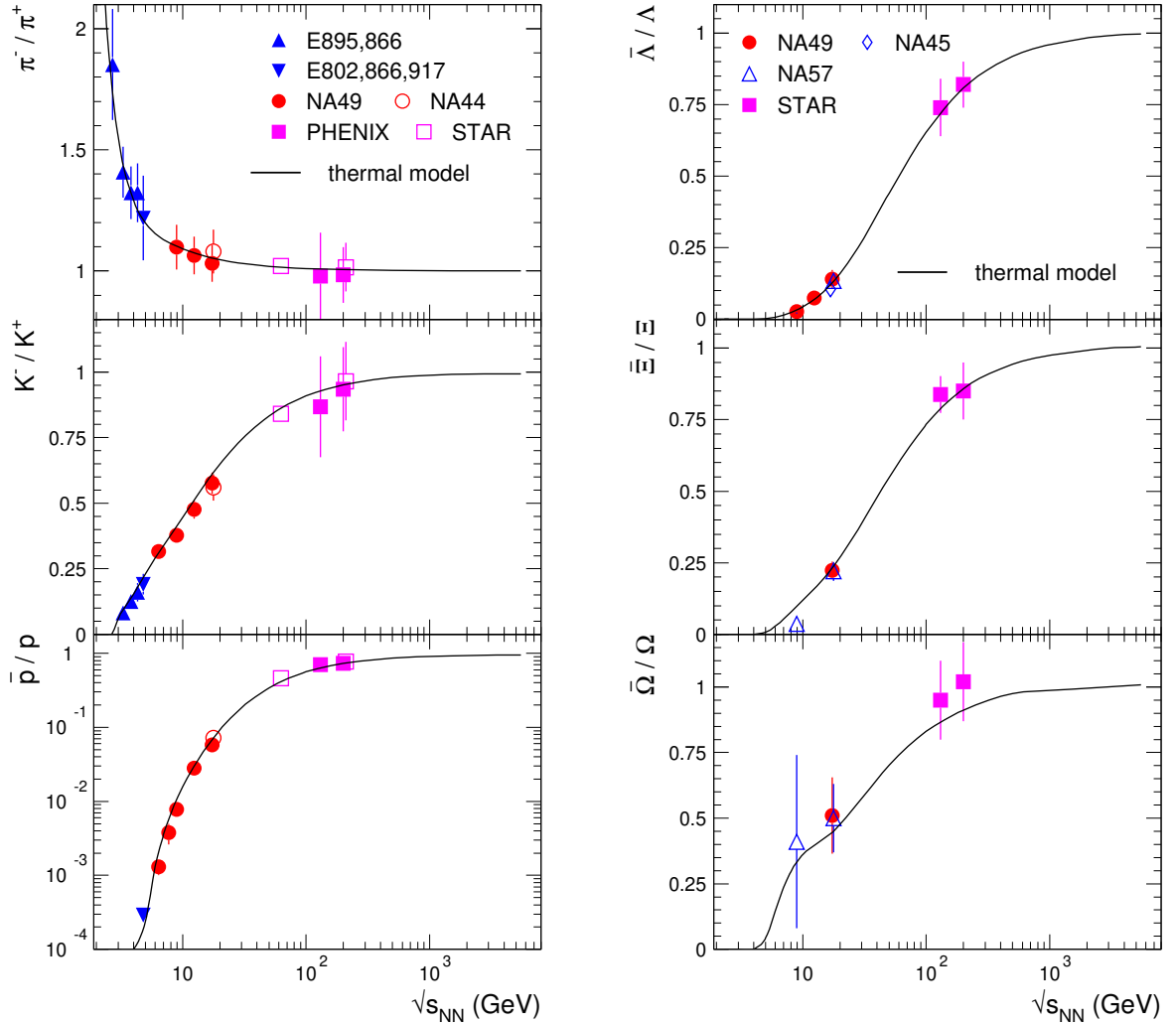


Fig. 16. The energy dependence of antiparticle/particle ratios.

is as well in agreement. The generally poor quality of thermal fits at SPS energies is not caused by ratios involving (multi)strange baryons.

The comparison of the measured and calculated excitation functions for hadron abundances with respect to pions is shown in Fig. 17. For a consistent comparison to the other measurements and to the calculations, the measured pion yield at $\sqrt{s_{NN}}=130$ GeV [70] was scaled assuming that 30% of the weak decays contribution was contained in the data (see above). The ratios shown in Fig. 17 have a very different energy dependence compared to those in Fig. 16, reflecting the evolution of the fireball composition at freeze-out as a function of energy. The step decrease of the p/π^+ ratio directly reflects the decrease as a function of energy of stopping of the incoming protons, implying a decrease of μ_b . The increase of pion production also plays a role in this ratio. Beyond $\sqrt{s_{NN}} \simeq 100$ GeV, the flattening is a consequence of the dominance of newly created baryons. The step variation of the K^+/π^+ and K^-/π^- ratios at the lowest energies reflects the threshold for strangeness production, determined in the model by the step increase of the temperature. The canonical suppression plays an important role as well. While the ratio K^-/π^-

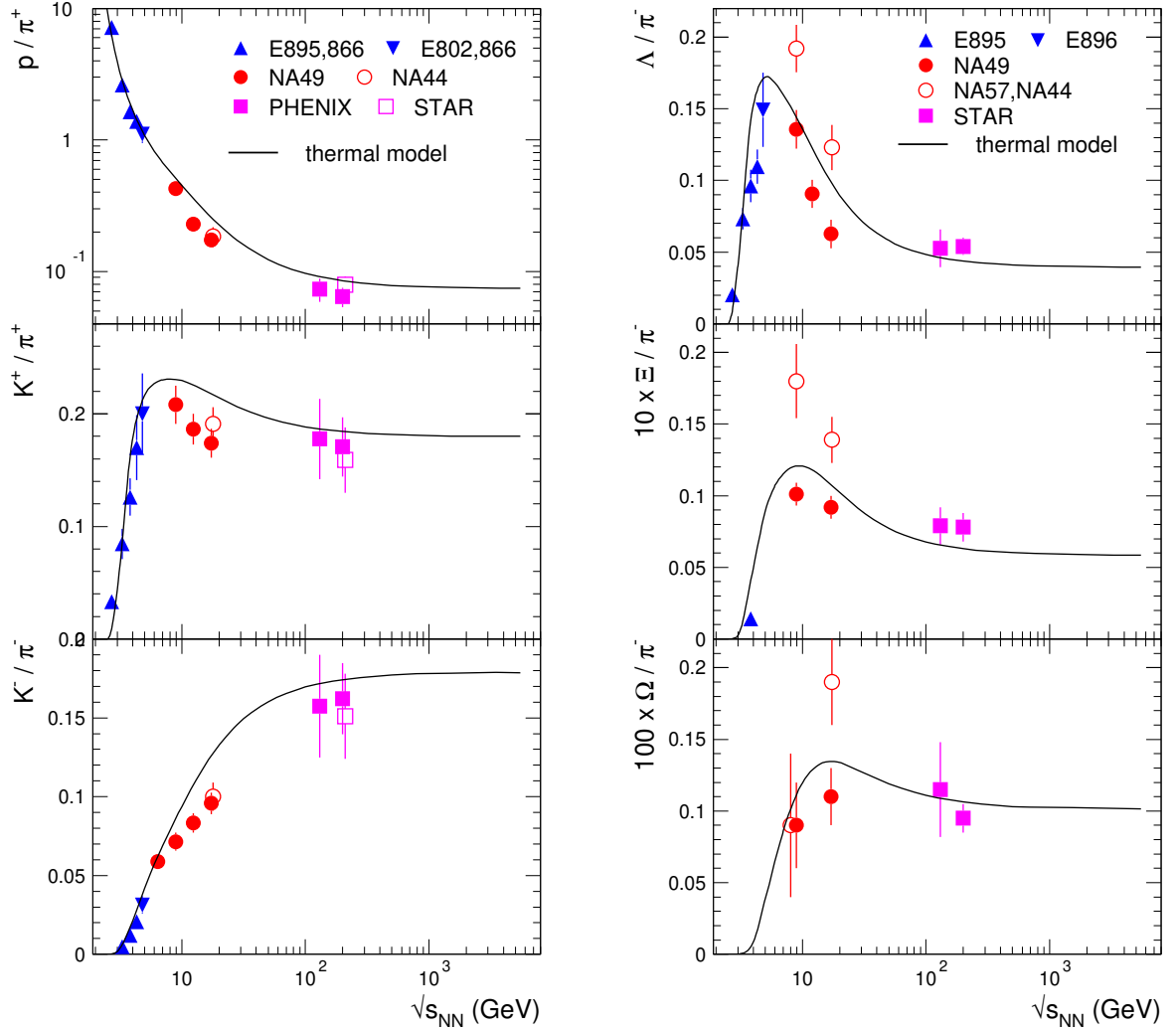


Fig. 17. The energy dependence of hadron yields relative to pions. In the right panel, note the scaling factors of 10 and 100 for the Ξ^-/π^- and Ω^-/π^- ratios, respectively.

shows a monotonic increase with energy, followed by a saturation, essentially determined by the temperature (as both particles are newly created), the ratio K^+/π^+ , which is much discussed as a signature for the onset of QGP [91–94], shows a characteristic broad peak around $\sqrt{s_{NN}} \simeq 8$ GeV. As the K^+ contains a u valence quark, which may come from the initial nucleons, its yield is the convolution of two competing contributions as a function of energy: i) the decreasing net light quark content and ii) the increasing production of quark-antiquark pairs. The peak in the K^+/π^+ ratio occurs naturally in the thermal model [26,25], but is broader and has to be seen in the context of other strange hadron yields [25] (right panel of Fig 17). It appears that, at the SPS energies of 80 and 158 AGeV, the yields of kaons and protons relative to pions are systematically below the thermal model predictions. We note that recent transport model calculations [93] grossly deviate from the measured K^+/π^+ ratio, while earlier results reproduced the data well [95]. We emphasize the good agreement between the two data sets (NA49 [58] and NA44 [57]) available at the top SPS energy.

The energy dependence of the relative hyperon yields, Λ/π^- , Ξ^-/π^- and Ω^-/π^- , shown in the right panel of Fig. 17, reveals the presence of characteristic peak structures, already noted in [26]. Their strength and location follows a mass hierarchy, recently discussed by Cleymans et al. [25]. The peaks are less pronounced and located at larger energies ($\sqrt{s_{NN}} \simeq 5, 10$ and 20 GeV) the more massive the hyperon species. This results from an interplay between the baryochemical potential (presence of the light quarks from the initial nucleons) and temperature. The agreement between the model and the data is good at AGS and RHIC energies, while at SPS the situation is more complex. The two available sets of data, NA49 [61–63] and NA57 [64], are in a clear disagreement: generally, the NA49 data are below the NA57 data. As a consequence of our adopted fitting procedure (see above) the model prediction is between the two data sets. We notice that the discrepancy of the data is manifest in the absolute yields: for instance, dN/dy of Λ at top SPS (5% central collisions) for NA49 and NA57 are 11.0 ± 1.6 and 18.5 ± 2.2 , respectively. The disagreement is well beyond the errors (statistical and systematic, added in quadrature) quoted by both experiments.

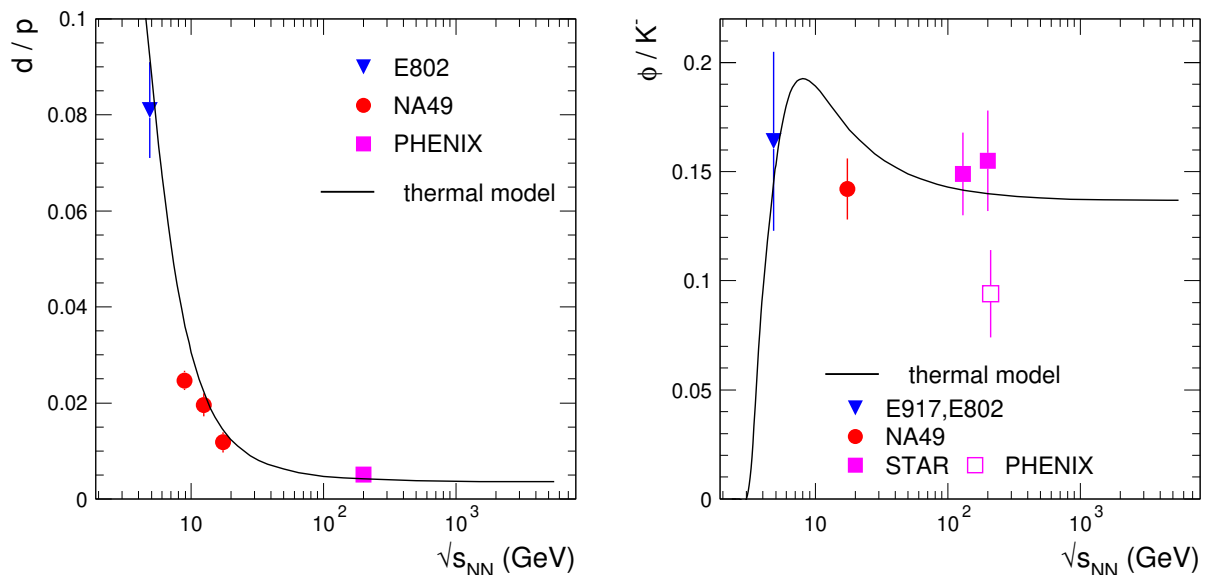


Fig. 18. The energy dependence of d/p and ϕ/K^- ratios.

In Fig. 18 we show the excitation function of the ratios d/p and ϕ/K^- . The ratio d/p shows a monotonic decrease as a function of energy, well explained by the model. The ratio ϕ/K^- shows a peak in the calculations, centered in this case at $\sqrt{s_{NN}} \simeq 8$ GeV. The model reproduces well the AGS measurement [55], while at SPS there is a disagreement. At RHIC the experimental situation is unclear; the model is in agreement with the STAR data.

Given the accuracy of the description of hadron ratios presented in the previous section, it is not surprising that, based on a parametrized energy dependence of T and μ_b , the model does reproduce the experimental values well over a broad energy range. However, systematic discrepancies between the model calculations and data are evident for the SPS data, in particular concerning the ratios involving strange to non-strange hadrons.

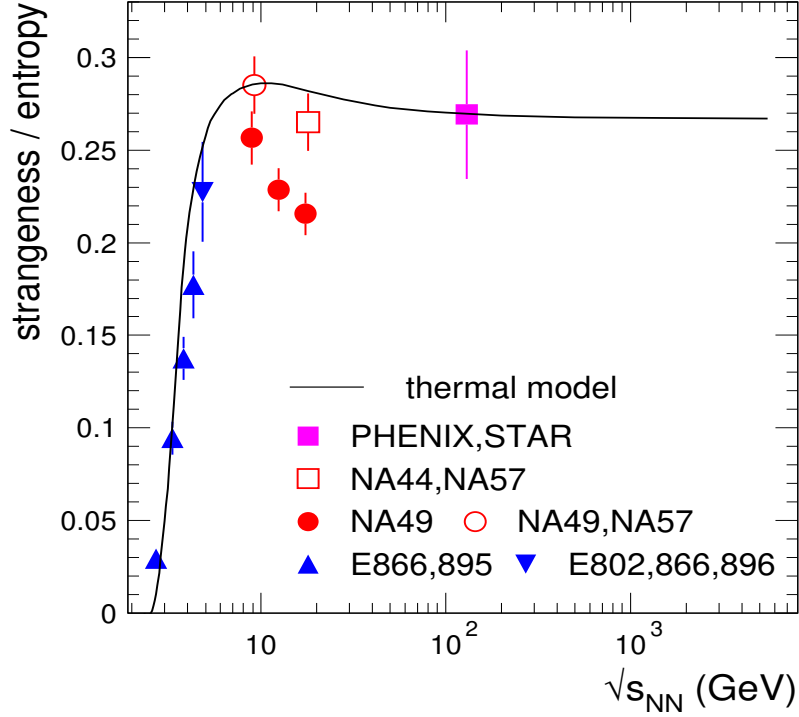


Fig. 19. Energy dependence of strangeness to entropy ratio (see text).

A more global way to represent the ratio of strange to non-strange hadrons is the strangeness (σ) to entropy (S) ratio. Its excitation function is presented in Fig. 19. We adopt an experiment-oriented construction of the two quantities, which we consistently employ for the model as well, calculated from the yields at mid-rapidity as:

$$\sigma = 2 \times (K^+ + K^-) + 1.54 \times (\Lambda + \bar{\Lambda}), \quad S = 1.5 \times (\pi^+ + \pi^-) + 2 \times \bar{p} \quad (8)$$

The strangeness has in principle to be complemented with the yields of ϕ , Ξ and Ω (and $\bar{\Xi}$ and $\bar{\Omega}$), but, since the measurements for these yields are scarce (as seen in Fig. 17 and 18), we have chosen to leave them out for the strangeness count. The factor 2 multiplying the kaon yields takes into account K^0 , while the factor 1.54 for Λ hyperons accounts for the contribution of Σ^\pm and was deduced from the model calculations.⁵ The factor 1.5 for the pion yields accounts for the π^0 yield, while in case of \bar{p} yields the factor 2 is used to account for the produced protons. As expected from the individual particle ratios studied above, the ratio strangeness/entropy is well reproduced by the model, with the exception of the data at SPS, where the NA49 data exhibit a sharper peak than predicted by the model. This feature is not supported by the NA57 data, which are in agreement with the model.

The results discussed above allow a rather confident prediction for hadron ratios in central

⁵ The yield of Σ^0 , which decays with 100% branching ratio into $\Lambda\gamma$, is always included in the Λ yield.

Table 3

Thermal model prediction for hadron ratios at LHC ($T=161$ MeV, $\mu_b=0.84$ MeV). No contribution from weak decays is included.

π^-/π^+	K^-/K^+	\bar{p}/p	$\bar{\Lambda}/\Lambda$	$\bar{\Xi}/\Xi$	$\bar{\Omega}/\Omega$
1.00	0.99	0.95	1.00	1.00	1.00
p/π^+	K^+/π^+	K^-/π^-	Λ/π^-	Ξ^-/π^-	Ω^-/π^-
0.074	0.180	0.179	0.039	0.0058	0.00106
ϕ/K^-	K^{*0}/K_S^0	Δ^{++}/p	$\Sigma(1385)^+/\Lambda$	Λ^*/Λ	$\Xi(1530)^0/\Xi^-$
0.136	0.312	0.216	0.140	0.075	0.396

Pb-Pb collisions at LHC energy [96], presented in Table 3. The antiparticle/particle ratios are all very close to unity, with the exception of \bar{p}/p , reflecting the small, but nonzero, μ_b value obtained from Eq. 7. Within the extrapolation scenario for the thermal parameters, the model predicts that the yields relative to pions are very similar to the values measured at the RHIC energy.

6 The phase diagram of hadronic matter

The values of T and μ_b obtained from our fits of the experimental data are shown in a phase diagram of hadronic and quark-gluon matter in Fig. 20. Full points are from fits of ratios of yields at midrapidity, open points are from fits of 4π ratios. An important observation about the phase diagram is that, for the 40 AGeV SPS energy and above, the thermal parameters agree with the phase boundary calculations from lattice QCD (LQCD) [12–14], implying that hadron yields are frozen at the phase boundary. The LQCD calculation [12] shown in Fig. 20 is for two light quarks (u, d) with realistic (close to physical) masses and a heavy strange quark. The critical temperature at $\mu_b=0$ from LQCD calculations is about 165 MeV [18] (and refs. therein), with a scale uncertainty of the order of 10 MeV [18,14] and with comparable systematic errors [18].

Also included in Fig. 20 are calculations of freeze-out curves for a hadron gas at constant energy density ($\varepsilon=500$ MeV/fm³) and at constant total baryon density ($n_b=0.12$ fm⁻³) [22]. The LQCD phase boundary calculated in [12] and shown in Fig. 20 apparently does not follow the expectation [13] (see also [97]) of a constant energy density dependence. However, depending on the method, the errors for the critical line from LQCD calculations can be large for finite μ_b [13].

The freeze-out points which are departing from the LQCD phase boundary are approximately described by the curve of a hadron gas at constant baryon density. An earlier proposed freeze-out criterion corresponds to an average energy per average number of hadrons of approximately 1 GeV [11]. It has also been argued recently that the freeze-out points can be described by a constant entropy density divided by T^3 [23]. This is a measure of the degrees of freedom; in a hadron gas with realistic masses the effective number of degrees of freedom depends explicitly on temperature and is not constant. As Cleymans et al. [25] have recently pointed out, for realistic excluded volume corrections,

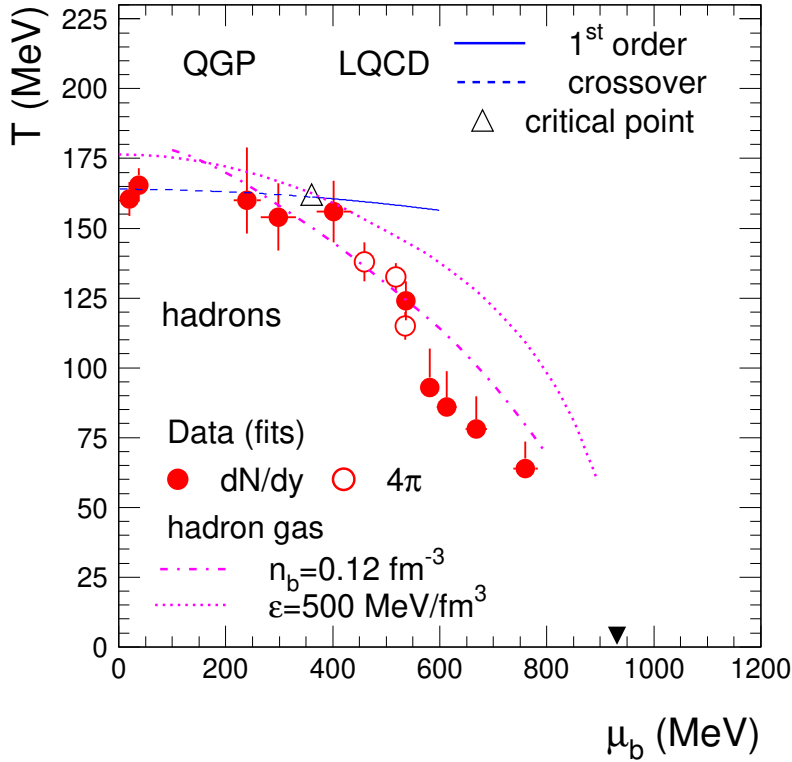


Fig. 20. The phase diagram of hadronic and quark-gluon matter in the T - μ_b plane. The experimental values for the chemical freeze-out are shown together with results of lattice QCD calculations [12]. The predicted [12] critical point is marked by the open triangle. Also included are calculations of freeze-out curves for a hadron gas at constant energy density ($\varepsilon=500$ MeV/fm³) and at constant total baryon density ($n_b=0.12$ fm⁻³). The full triangle indicates the location of ground state nuclear matter (atomic nuclei).

this criterion grossly deviates from the freeze-out points. A comparison of various freeze-out criteria was recently done in ref. [24], which showed that all are identical except for large and small μ_b values. All are smooth curves and consequently not consistent with the new results presented here, which exhibit a rather steep trend at intermediate μ_b values. However, the errors need to be improved before one can confidently rule out any (smooth) universal freeze-out criterion. An exciting possibility is that the rather abrupt turn-over in the freeze-out points near $\mu_b=400$ MeV is caused by the approach to the QCD phase boundary.

The underlying assumption of the thermal model used to extract the (T, μ_b) values is equilibrium at chemical freeze-out. A natural question then is how the equilibrium is achieved? The answer obviously cannot come from within the framework of the thermal model. Considerations about collisional rates and timescales of the hadronic fireball expansion imply that at SPS and RHIC the equilibrium cannot be established in the hadronic medium below the critical temperature T_c [15,16]. In a recent paper [16] many body collisions near T_c were investigated as a possible mechanism for the equilibration within the hadronic stage. There it is argued that because of the rapid density change near a phase transition such multi-particle collisions provide a natural explanation for the observation of chemical equilibration at RHIC energies and lead to $T = T_c$ to within an accuracy of a few MeV. While this argument is expected to be valid also for SPS energies, the situation at lower energies needs further consideration.

The critical temperature determined from RHIC and SPS data assuming $T \approx T_c$ coincides well with lattice estimates [12,14,18]. These arguments buttress the conclusion that the

hadrochemical freeze-out parameters probe experimentally in a unique manner the critical line of the QCD phase transition between hadrons and QGP [98]. Despite the rather large systematic errors of the extracted temperature for the SPS energies, our results imply that the phase boundary is reached for beam energies around 40 AGeV. The experimental data at 20 AGeV [89] will constrain further this energy range.

Based on the LQCD results of Fodor and Katz [12] shown in Fig. 20, the experimental freeze-out points at SPS are located in the vicinity of the critical point. It was pointed out recently [19] that the existence of a critical point for $\mu_b < 500$ MeV requires a fine tuning of the (light) quarks masses within 5%. However, it is important to recognize that serious open problems of LQCD [19] need to be solved before one could address quantitatively such a delicate possibility. Nevertheless, it is interesting to speculate whether the deviations from the thermal model (including rather poor-quality fits) which we have encountered for the SPS energies are a hint for the critical point. It is expected that, in the (broad) vicinity of the critical (end)point the thermal model would not work [68]. Thermal fits including fluctuations have been already performed for the top SPS energy [69]. Unfortunately, the present experimental situation, namely the level of disagreement between data, does not allow any firm conclusion on the interesting issue of the critical point.

7 Summary

We have analyzed the experimental hadron yields ratios over a broad energy range ($\sqrt{s_{NN}}=2.7-200$ GeV) in comparison with thermal model calculations. The fits of the experimental data with the model provide the temperature and baryo-chemical potential, at hadrochemical freeze-out. The quality of the fits is very good for most cases, providing support for the validity of the approach. From our analysis we have established parametrizations of T and μ_b as a function of energy. This allows to assess and understand trends visible in the experimental data. In particular, we have discussed for the yields of strange and multi-strange hadron yields relative to pions the resulting non-monotonic energy dependence, which describes the main features observed in the data, but not the details. Furthermore, we have provided quantitative predictions for hadron ratios at $\sqrt{s_{NN}}=62.4$ GeV and at LHC energy, where first data are expected soon. The analysis presented here has also led to an updated version of the chemical freeze-out curve. The results buttress previous observations that, from $\sqrt{s_{NN}} \approx 10$ GeV on, the chemical freeze-out points coincide with the phase boundary between hadrons and the QGP as predicted by solving QCD on the lattice. We have provided chemical freeze-out points, for the first time, at the 4 low AGS energies. In this energy range the freeze-out curve exhibits a peculiar and intriguing structure which needs further explanation.

Appendix

In this Appendix we discuss technical aspects related to the thermal model analysis. First, we concentrate on the technical aspects of fitting yields rather than ratios, and the demonstration that both methods produce equivalent results. Secondly, we briefly address

the issue of the role of γ_S in the thermal model fits. Finally, we comment on the issue of weak feeding. The absolute yields (and consequently the values for the volume) quoted here are for $N_{part}=350$.

A. Analysis of particle yields

The fit of mid-rapidity yields for the top ASG energy is shown in Fig. 21. The resulting parameters are: $T=132$ MeV, $\mu_b=546$ MeV, $V=900$ fm³. With $\chi^2/N_{df}=10.3/7$, the fit is good. The temperature is somewhat higher than the temperature obtained when fitting ratios. Excluding from the fit the yields of \bar{p} , $\bar{\Lambda}$, ϕ , and d one obtains: $T=110$ MeV, $\mu_b=550$ MeV, $V=2620$ fm³, $\chi^2/N_{df}=1.2/3$. The resulting change in T is 20%, larger than the difference derived from the fit of ratios (15%). This lower temperature is "compensated" by an unphysically large volume, leading to a good fit in this case too. The main contribution to this effect arises from the absence of \bar{p} and $\bar{\Lambda}$ (when fitting without \bar{p} and $\bar{\Lambda}$: $T=114$ MeV, $\mu_b=551$ MeV, $V=2100$ fm³, $\chi^2/N_{df}=2.8/5$).

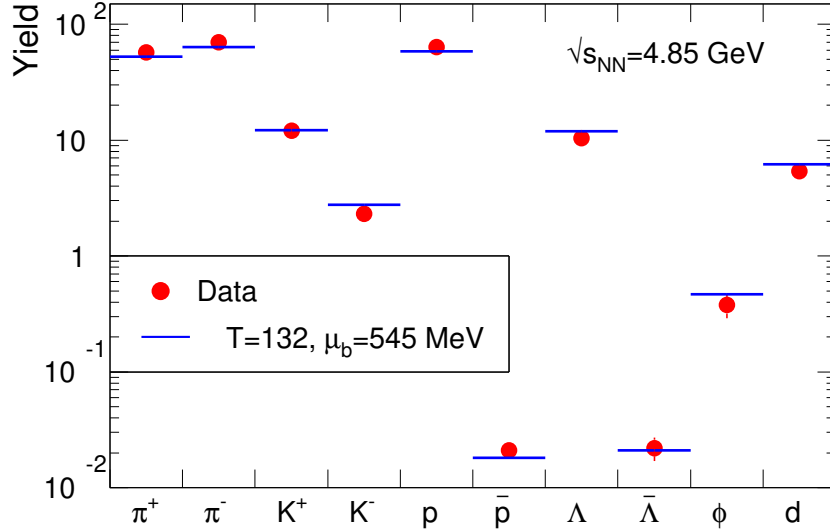


Fig. 21. Hadron yields at mid-rapidity and the best fit for the top AGS energy.

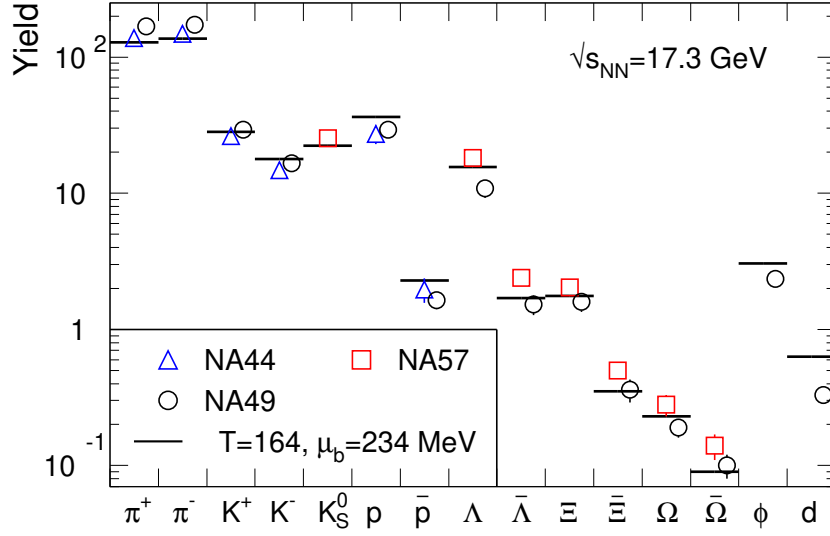
Our fits of (mid-rapidity) yields at lower AGS energies result in identical values for T and μ_b as when using ratios. The extracted volume is much larger than for the top AGS energy. This originates in the bias of the temperature due to the limited set of particle yields available, as discussed above and as also observed when fitting ratios. Based on the above results at top AGS energy, we conclude that the extracted volume at the lower energies is overestimated by a factor of 2.9.

The comparison of mid-rapidity yields and the best fit for the top SPS energy is shown in Fig. 22. The temperature is slightly higher than in case of ratios, but this is within 1- σ errors. The discrepancy between different data sets noted in case of ratios is evident also

Table 4

Summary of the results of the fits using mid-rapidity yields at top SPS energy.

data set	T (MeV)	μ_b (MeV)	V (fm ³)	χ^2/N_{df}	T (MeV)	μ_b (MeV)	V	δ^2
NA44+NA57	174	240	750	24.2/10	174	240	750	0.28
NA49	158	231	1250	56.2/10	160	225	1150	0.44
combined	164	234	1000	105/23	168	234	900	1.10

Fig. 22. Mid-rapidity yields and best fit (combined data) at the SPS beam energy of 158 AGeV (d was not included in the fit).

for the yields. As for the ratios, this leads to contradictory results when fitting the data separately, see Table 4. The quality of the fits is for all SPS energies significantly poorer than in case of ratios.

At the RHIC energy of $\sqrt{s_{NN}}=130$ GeV, Fig. 23, the resulting temperature from the fits of absolute yields is slightly higher than in case of ratios. This, as well as a poorer $\chi^2/N_{df}=15.3/10$, is mainly due to an apparent experimental upward bias of the yield of the Ξ (and, to a lesser extent, Λ) hyperons. Without Ξ 's in the fit: $T=160$ MeV, $\mu_b=32$ MeV, $V=2200$ fm³, $\chi^2/N_{df}=4.3/8$.

The main results for the best fits of absolute hadron yields are summarized in Table 5. The upper part in Table 5 is for the fits using mid-rapidity data, the lower part is for data integrated over 4π . The fits of yields give similar temperatures as for ratios, but larger values for baryo-chemical potentials and larger χ^2 values. One notices that, in general, χ^2/N_{df} is close to or below unity, being significantly above unity only for the SPS energies, as for the case using ratios of yields. For all energies, the χ^2 values are larger than in case of the fits of ratios. This is expected, as part of the discrepancy between data and model is cancelled in the ratios, for instance in case of antiparticle/particle ratios. These results

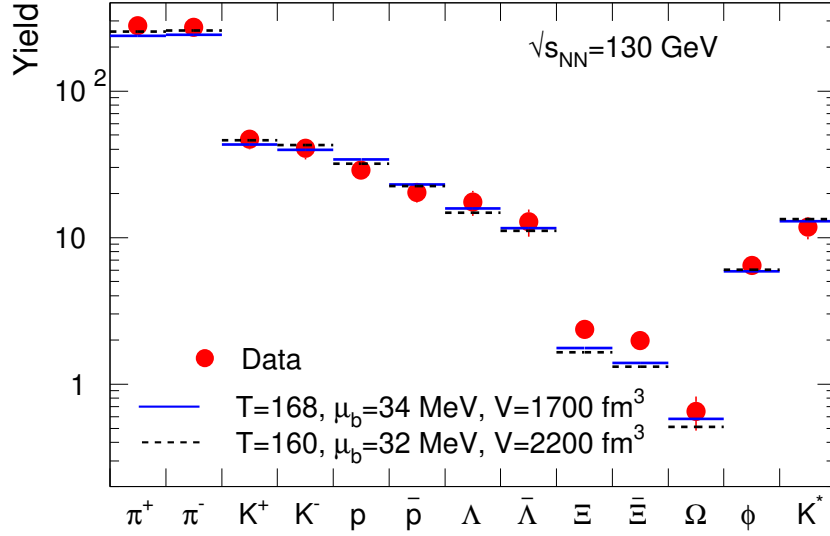


Fig. 23. Hadron yields with best fit at $\sqrt{s_{NN}}=130$ GeV. The dashed lines are for the best fit excluding the Ξ hyperons. The Ω yield includes both Ω and $\bar{\Omega}$.

demonstrate that the use of ratios is less prone to biases. This is one of the reasons why we prefer to fit particle ratios rather than yields.

B. Inclusion of γ_S into the fits

In Table 6, we present results obtained with mid-rapidity and 4π -integrated yields with a thermal model including a strangeness suppression factor γ_S . The results for the mid-rapidity data demonstrate that the key quantities, namely T and μ_b , are very little influenced by whether or not γ_S is included as a fit parameter. Also, the quality of the fits is not significantly improved by including γ_S .

The fits of 4π yields including γ_S leads to a substantial improvement of the fit quality only for the higher SPS energies, but still the fit seldom attains a good quality. For these energies, the resulting T (and also μ_b) values are larger than in the case without γ_S (Table 5). This effect is negligible for the lowest SPS energy and increases gradually as a function of energy, see Table 6. This is illustrated in Fig. 24 for the lowest and highest SPS beam energies. Contrary to expectations, the volume and γ_S show a non-monotonic behavior as a function of energy (also apparent in the analysis of Becattini et al. [20]). In view of this, we regard V and γ_S as compensatory parameters for an inadequate fit of 4π data. As a consequence, the fact that the temperatures from the fits of 4π data using γ_S are very similar to those extracted from fits of mid-rapidity data should be viewed as a coincidence.

Table 5

Summary of the results of the thermal fits of yields. The upper part shows the results obtained using mid-rapidity data, the lower part is for data integrated over 4π .

$\sqrt{s_{NN}}$ (GeV)	T	μ_b	V	χ^2/N_{df}	T	μ_b	V	δ^2	ΔT	$\Delta\mu_b$	ΔV
2.70	64	760	5880	1.19/2	64	760	5900	0.013	+13,-2	23	140
3.32	78	669	6280	0.54/3	78	670	6200	0.003	+16,-3	20	230
3.84	88	610	5290	1.62/3	88	610	5200	0.020	+18,-3	19	220
4.30	94	588	4940	1.5/3	96	575	4400	0.026	+19,-3	17	540
4.85	132	546	900	10.3/7	132	540	900	0.13	4	11	170
8.76	154	382	850	51/13	160	418	700	0.69	6	36	250
12.3	150	277	1300	47/5	152	265	1300	0.18	5	12	300
17.3	164	234	1000	105/23	168	234	900	1.10	6	11	250
130	168	34	1700	15.3/10	170	34	1600	0.24	4	6	220
6.27	128	489	3850	15.9/4	128	453	4200	0.10	3	36	450
7.62	138	471	3450	27/4	142	474	2900	0.22	4	13	550
8.76	136	426	4600	56/6	140	366	4100	0.60	5	60	500
12.3	146	373	5400	61/4	148	298	4800	0.30	6	75	750
17.3	148	228	6100	64/9	152	210	5700	0.51	5	22	650

Table 6

Results of the fits of yields using γ_S . The upper part is for mid-rapidity data, the lower part is for 4π data.

$\sqrt{s_{NN}}$ (GeV)	T	μ_b	V	γ_S	χ^2/N_{df}	T	μ_b	V	γ_S	δ^2
8.76	156	386	800	0.94	48/12	160	414	700	0.95	0.59
12.3	144	265	1900	0.84	32/4	152	265	1300	0.93	0.18
17.3	162	231	1100	0.96	102/23	168	231	900	1.0	1.12
6.27	132	480	3600	0.83	9.0/3	128	450	4300	0.94	0.10
7.62	140	448	3850	0.81	10.6/3	142	444	3550	0.75	0.08
8.76	152	418	3000	0.74	7.0/5	152	418	3200	0.69	0.04
12.3	162	340	3400	0.71	5.9/3	158	322	4000	0.70	0.023
17.3	162	267	4600	0.76	17.6/8	162	258	4300	0.84	0.85

C. Importance of feed-down from weakly decaying states

In Fig. 25 we show, as a function of energy, the contribution of weak decays to the yields of pions, protons and Λ hyperons calculated with the parametrizations for T and μ_b (Eqs. 6 and 7 in Section 4). Shown is the fraction of the total yield of these particles originating from weak decays. This fraction reaches the asymptotic values of 15%, 25% and 35% for π , Λ and p , respectively, being significantly larger in case of antiparticles at AGS and SPS

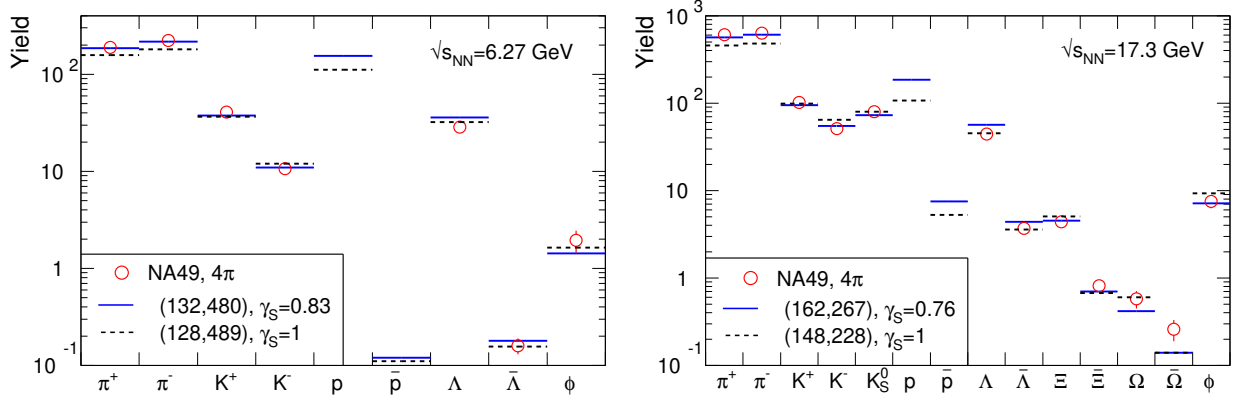


Fig. 24. Hadron yields integrated over 4π with best fits with (continuous lines) and without (dashed lines) γ_S at the SPS energies of 20 and 158 AGeV.

energies. Since this contribution is sizeable, a consistent comparison between data and model is required.

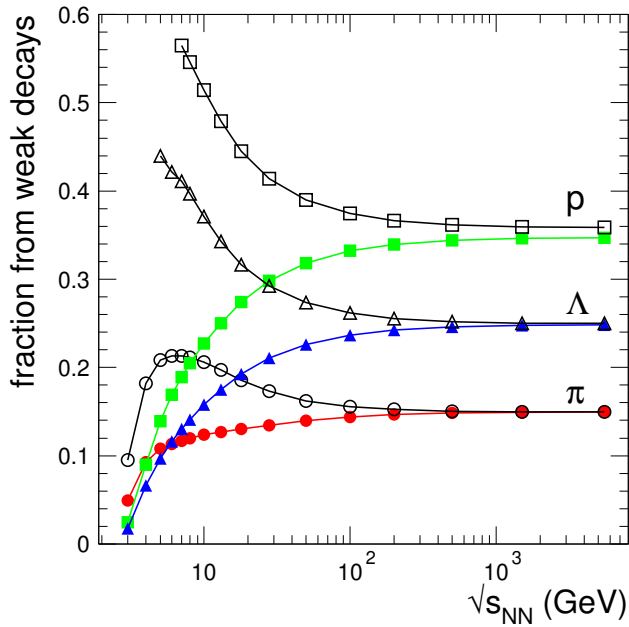


Fig. 25. The energy dependence of the fraction of total hadron yields originating from weak decays. The full symbols are for particles (π^+ , p , Λ), the open ones for antiparticles (π^- , \bar{p} , $\bar{\Lambda}$).

References

- [1] P. Braun-Munzinger, K. Redlich, J. Stachel, in *Quark Gluon Plasma 3*, Eds. R. Hwa, X.-N. Wang, (World Scientific, Singapore, 2004) p. 491 [nucl-th/0304013].
- [2] P. Braun-Munzinger, J. Stachel, J.P. Wessels, N. Xu, Phys. Lett. B344 (1995) 43 [nucl-th/9410026], Phys. Lett. B365 (1996) 1 [nucl-th/9508020].

- [3] J. Cleymans, D. Elliott, A. Keranen, E. Suhonen, Phys. Rev. C 57 (1998) 3319 [nucl-th/9711066]; J. Cleymans, H. Oeschler, K. Redlich, Phys. Rev. C 59 (1999) 1663 [nucl-th/9809027].
- [4] R. Averbeck, R. Holzmann, V. Metag, R.S. Simon, Phys. Rev. C 67 (2003) 024903 [nucl-ex/0012007].
- [5] P. Braun-Munzinger, I. Heppe, J. Stachel, Phys. Lett. B 465 (1999) 15 [nucl-th/9903010].
- [6] P. Braun-Munzinger, D. Magestro, K. Redlich, J. Stachel, Phys. Lett. B 518 (2001) 41 [nucl-th/0105229].
- [7] W. Broniowski, W. Florkowski, M. Michalec, Acta Phys. Polon. B33 (2002) 761 [nucl-th/0106009]; W. Broniowski, W. Florkowski, Phys. Rev. C 65 (2002) 064905 [nucl-th/0112043].
- [8] M. Kaneta, N. Xu, nucl-th/0405068.
- [9] J. Adams et al. (STAR), Nucl. Phys. A 757 (2005) 102 [nucl-ex/0501009].
- [10] P. Braun-Munzinger, J. Stachel, Nucl. Phys. A 638 (98) 3c [nucl-ex/9803015].
- [11] J. Cleymans, K. Redlich, Phys. Rev. Lett. 81 (1998) 5284 [nucl-th/9808030]; Phys. Rev. C 60 (1999) 054908 [nucl-th/9903063].
- [12] Z. Fodor, S.D. Katz, JHEP 404 (2004) 50 [hep-lat/0402006].
- [13] C.R. Allton, S. Ejiri, S.J. Hands, O. Kaczmarek, F. Karsch, E. Laermann, Ch. Schmidt, L. Scorzato, Phys. Rev. D 66 (2002) 074507 [hep-lat/0204010].
- [14] P. de Forcrand, O. Philipsen, Nucl. Phys. B 642 (2002) 290 [hep-lat/0205016].
- [15] R. Stock, Phys. Lett. B 456 (1999) 277 [hep-ph/9905247].
- [16] P. Braun-Munzinger, J. Stachel, Ch. Wetterich, Phys. Lett. B 596 (2004) 61 [nucl-th/0311005].
- [17] M.A. Stephanov, Prog. Theor. Phys. Suppl. 153 (2004) 139 [hep-ph/0402115].
- [18] F. Karsch, J. Phys. G 31 (2005) S633 [hep-lat/0412038].
- [19] O. Philipsen, PoS LAT2005 (2005) 016 [hep-lat/0510077].
- [20] F. Becattini, M. Gaździcki, A. Keranen, J. Manninen, R. Stock, Phys. Rev. C 69 (2004) 024905 [hep-ph/0310049]; J. Manninen, F. Becattini, M. Gaździcki, hep-ph/0511092.
- [21] J. Letessier, J. Rafelski, nucl-th/0504028.
- [22] P. Braun-Munzinger, J. Stachel, J. Phys. G 28 (2002) 1971 [nucl-th/0112051] (see also P. Braun-Munzinger, nucl-ex/0508024).
- [23] A. Tawfik, hep-ph/0410392.
- [24] J. Cleymans, H. Oeschler, K. Redlich, S. Wheaton, hep-ph/0511094.
- [25] J. Cleymans, H. Oeschler, K. Redlich, S. Wheaton, Phys. Lett. B 615 (2005) 50 [hep-ph/0411187].
- [26] P. Braun-Munzinger, J. Cleymans, H. Oeschler, K. Redlich, Nucl. Phys. A 697 (2002) 902 [hep-ph/0106066].

- [27] F. Becattini, G. Passaleva, Eur. Phys. J. C 23 (2002) 551 [hep-ph/0110312].
- [28] A. Andronic, P. Braun-Munzinger, K. Redlich, Nucl. Phys. A 765 (2006) 211 [nucl-th/0506083].
- [29] S. Eidelman et al., Phys. Lett. B 592 (2004) 1.
- [30] F. Karsch, K. Redlich, A. Tawfik, Eur. Phys. J. C 29 (2003) 549 [hep-ph/0303108], Phys. Lett. B 571 (2003) 50 [hep-ph/0306208].
- [31] M. Michalec, W. Florkowski, W. Broniowski, Phys. Lett. B 520 (2001) 213 [nucl-th/0103029].
- [32] D. Zschesche, S. Schramm, J. Schaffner-Bielich, H. Stöcker, W. Greiner, Phys. Lett. B 547 (2002) 7 [nucl-th/0209022].
- [33] G.E. Brown, M. Rho, Phys. Rep. 363 (2002) 85.
- [34] V. Koch, J. Phys. G 30 (2004) S41 [nucl-th/0306037].
- [35] W. Weinhold, B. Friman, W. Nörenberg, Phys. Lett. B 433 (1998) 236 [nucl-th/9710014].
- [36] D.H. Rischke, M.I. Gorenstein, H. Stöcker, W. Greiner, Z. Phys. C 51 (1991) 485.
- [37] G.D. Yen, M.I. Gorenstein, W. Greiner, S.N. Nang, Phys. Rev. C 56 (1997) 2210 [nucl-th/9711062].
- [38] F. Becattini, Z. Phys. C 69 (1996) 485; F. Becattini, U. Heinz, Z. Phys. C 76 (1997) 269 [hep-ph/9702274].
- [39] J. Cleymans, K. Redlich, E. Suhonen, Z. Phys. C 51 (1991) 137.
- [40] G. Torrieri et al., Comp. Phys. Comm. 167 (2005) 229 [nucl-th/0404083].
- [41] S. Wheaton, J. Cleymans, hep-ph/0407174.
- [42] A. Kisiel, T. Taluc, W. Broniowski, W. Florkowski, Comp. Phys. Comm. 174 (2006) 669 [nucl-th/0504047].
- [43] D. Miśkowiec, private communication (<http://www.gsi.de/~misko/overlap/>).
- [44] L.V. Bravina et al., Phys. Rev. C 60 (1999) 024904 [hep-ph/9906548].
- [45] J.L. Klay et al. (E895), Phys. Rev. Lett. 88 (2002) 102301; J.L. Klay, PhD Thesis, UC Davis (2001).
- [46] B.B. Back et al. (E917), Phys. Rev. Lett. 86 (2001) 1970 [nucl-ex/0003007].
- [47] J.L. Klay et al. (E895), Phys. Rev. C 68 (2003) 054905 [nucl-ex/0306033].
- [48] L. Ahle et al. (E866/E917), Phys. Lett. B 476 (2000) 1 [nucl-ex/9910008]; Phys. Lett. B 490 (2000) 53 [nucl-ex/0008010].
- [49] C. Pinkenburg et al. (E895), Nucl. Phys. A 698 (2002) 495c [nucl-ex/0104025].
- [50] P. Chung et al. (E895), Phys. Rev. Lett. 91 (2003) 202301 [nucl-ex/0302021].
- [51] J. Barrette et al. (E877), Phys. Rev. C 62 (2000) 024901 [nucl-ex/9910004].
- [52] L. Ahle et al. (E802), Phys. Rev. C 60 (1999) 064901.
- [53] L. Ahle et al. (E802), Phys. Rev. C 58 (1998) 3523.

- [54] S. Albergo et al. (E896) Phys. Rev. Lett. 88 (2002) 062301.
- [55] B.B. Back et al. (E917), Phys. Rev. C 69 (2004) 054901 [nucl-ex/0304017].
- [56] B.B. Back et al. (E917), Phys. Rev. Lett. 87 (2001) 1970.
- [57] I.G. Bearden et al. (NA44), Phys. Rev. C 66 (2002) 044907 [nucl-ex/0202019].
- [58] S.V. Afanasiev et al. (NA49), Phys. Rev. C 66 (2002) 054902 [nucl-ex/0205002].
- [59] S.V. Afanasiev et al. (NA49), Phys. Rev. C 69 (2004) 024902.
- [60] C. Alt et al. (NA49), nucl-ex/0512035.
- [61] T. Anticic et al. (NA49), Phys. Rev. Lett. 93 (2004) 022302 [nucl-ex/0311024].
- [62] S.V. Afanasiev et al. (NA49), Phys. Lett. B 538 (2002) 275 [nucl-ex/9810005].
- [63] C. Alt et al. (NA49), Phys. Rev. Lett. 94 (2005) 192301 [nucl-ex/0409004].
- [64] F. Antinori et al. (NA57), Phys. Lett. B 595 (2004) 68 [nucl-ex/0403022].
- [65] F. Antinori et al. (NA57), J. Phys. G 31 (2005) 1345 [nucl-ex/0509009].
- [66] S.V. Afanasiev et al. (NA49), Phys. Lett. B 491 (2000) 59.
- [67] H. Bøggild, private communication.
- [68] C. Nonaka, M. Asakawa, Phys. Rev. C 71 (2005) 044904 [nucl-th/0410078]; M. Asakawa, C. Nonaka, nucl-th/0509091.
- [69] A. Dumitru, L. Portugal, D. Zschesche, Phys. Rev. C 73 (2006) 024902 [nucl-th/0511084].
- [70] K. Adcox et al. (PHENIX), Phys. Rev. Lett. 88 (2002) 242301 [nucl-ex/0112006], and Phys. Rev. C 69 (2004) 024904 [nucl-ex/0307010].
- [71] K. Adcox et al. (PHENIX), Phys. Rev. Lett. 89 (2002) 092302 [nucl-ex/0204007].
- [72] J. Adams et al. (STAR), Phys. Rev. Lett. 92 (2004) 182301 [nucl-ex/0307024].
- [73] J. Adams et al. (STAR), Phys. Lett. B 567 (2003) 167 [nucl-ex/0206008].
- [74] C. Adler et al. (STAR), Phys. Rev. C 65 (2002) 041901(R).
- [75] C. Adler et al. (STAR), Phys. Rev. C 66 (2002) 061901 [nucl-ex/0205015].
- [76] S.S. Adler et al. (PHENIX), Phys. Rev. C 69 (2004) 034909 [nucl-ex/0307022].
- [77] J. Adams et al. (STAR), Phys. Rev. Lett. 92 (2004) 112301 [nucl-ex/0310004].
- [78] I. Arsene et al. (BRAHMS), Phys. Rev. C 72 (2005) 014908 [nucl-ex/0503010].
- [79] J. Adams et al. (STAR), Phys. Lett. B 612 (2005) 181 [nucl-ex/0406003].
- [80] S.S. Adler et al. (PHENIX), Phys. Rev. C 72 (2005) 014903 [nucl-ex/0410012].
- [81] J. Adams et al. (STAR), Phys. Rev. C 71 (2005) 064902 [nucl-ex/0412019].
- [82] S.S. Adler et al. (PHENIX), Phys. Rev. Lett. 94 (2005) 122302 [nucl-ex/0406004].
- [83] A. Billmeier et al. (STAR), J. Phys. G 30 (2004) S363.

- [84] H. Zhang (STAR), nucl-ex/0403010.
- [85] O. Barannikova (STAR), nucl-ex/0403014.
- [86] C. Markert et al. (STAR), J. Phys. G 31 (2005) S169 [nucl-ex/0503013].
- [87] D. Adamova et al. (CERES), Phys. Rev. Lett. 90 (2003) 022301 [nucl-ex/0207008]; for a recent review, see M. Lisa, S. Pratt, R. Soltz, U. Wiedemann, Ann. Rev. Nucl. Part. Sci. 55 (2005) 357 [nucl-ex/0505014].
- [88] L. Ruan et al. (STAR), J. Phys. G 31 (2005) S1029 [nucl-ex/0503015].
- [89] V. Friese (NA49), J. Phys. G 31 (2005) S911 [nucl-ex/0412013]; see the compilation of NA49 data available at:
http://na49info.cern.ch/na49/Archives/Data/NA49NumericalResults/na49_compil.pdf
- [90] A. Marín (NA45/CERES), J. Phys. G 30 (2004) S709 [nucl-ex/0406007].
- [91] M. Gaździcki, M.I. Gorenstein, Acta Phys. Polon. B30 (1999) 2705 [hep-ph/9803462].
- [92] M. Gaździcki, J. Phys. G 30 (2004) S161 [hep-ph/0305176].
- [93] E. Bratkovskaya et al., Phys. Rev. C 69 (2004) 054907 [nucl-th/0402026].
- [94] V. Koch, A. Majumder, J. Randrup, Phys. Rev. C 72 (2005) 064903 [nucl-th/0509030].
- [95] F. Wang, H. Liu, H. Sorge, N. Xu, J. Yang, Phys. Rev. C 61 (2000) 064904 [nucl-th/9909001].
- [96] P. Braun-Munzinger, Nucl. Phys. A 661 (1999) 261c [nucl-ex/9908007].
- [97] A. Tawfik, Phys. Rev. D 71 (2005) 054502 [hep-ph/0412336].
- [98] J. Stachel, nucl-ex/0510077.